NASA/TP—2001–211274

Prospects For Nuclear Electric Propulsion Using Closed-Cycle Magnetohydrodynamic Energy Conversion

R.J. Litchford, L.J. Bitteker, and J.E. Jones
Marshall Space Flight Center, Marshall Space Flight Center, Alabama

October 2001

The NASA STI Program Office…in Profile

Since its founding, NASA has been dedicated to the advancement of aeronautics and space science. The NASA Scientific and Technical Information (STI) Program Office plays a key part in helping NASA maintain this important role.

The NASA STI Program Office is operated by Langley Research Center, the lead center for NASA's scientific and technical information. The NASA STI Program Office provides access to the NASA STI Database, the largest collection of aeronautical and space science STI in the world. The Program Office is also NASA's institutional mechanism for disseminating the results of its research and development activities. These results are published by NASA in the NASA STI Report Series, which includes the following report types:

- TECHNICAL PUBLICATION. Reports of completed research or a major significant phase of research that present the results of NASA programs and include extensive data or theoretical analysis. Includes compilations of significant scientific and technical data and information deemed to be of continuing reference value. NASA's counterpart of peer-reviewed formal professional papers but has less stringent limitations on manuscript length and extent of graphic presentations.

- TECHNICAL MEMORANDUM. Scientific and technical findings that are preliminary or of specialized interest, e.g., quick release reports, working papers, and bibliographies that contain minimal annotation. Does not contain extensive analysis.

- CONTRACTOR REPORT. Scientific and technical findings by NASA-sponsored contractors and grantees.

- CONFERENCE PUBLICATION. Collected papers from scientific and technical conferences, symposia, seminars, or other meetings sponsored or cosponsored by NASA.

- SPECIAL PUBLICATION. Scientific, technical, or historical information from NASA programs, projects, and mission, often concerned with subjects having substantial public interest.

- TECHNICAL TRANSLATION. English-language translations of foreign scientific and technical material pertinent to NASA's mission.

Specialized services that complement the STI Program Office's diverse offerings include creating custom thesauri, building customized databases, organizing and publishing research results…even providing videos.

For more information about the NASA STI Program Office, see the following:

- Access the NASA STI Program Home Page at ***http://www.sti.nasa.gov***

- E-mail your question via the Internet to help@sti.nasa.gov

- Fax your question to the NASA Access Help Desk at (301) 621–0134

- Telephone the NASA Access Help Desk at (301) 621–0390

- Write to:
  NASA Access Help Desk
  NASA Center for AeroSpace Information
  7121 Standard Drive
  Hanover, MD 21076–1320
  (301)621–0390

NASA/TP—2001–211274

Prospects For Nuclear Electric Propulsion Using Closed-Cycle Magnetohydrodynamic Energy Conversion

R.J. Litchford, L.J. Bitteker, and J.E. Jones
Marshall Space Flight Center, Marshall Space Flight Center, Alabama

National Aeronautics and
Space Administration

Marshall Space Flight Center • MSFC, Alabama 35812

October 2001

Acknowledgments

This work was sponsored by the Advanced Propulsion Research Project Office, Advanced Space Transportation Program, George C. Marshall Space Flight Center (MSFC), National Aeronautics and Space Administration. The authors acknowledge and thank Tara Poston (MSFC/TD30) for her expert assistance with the trajectory analyses.
The first author expresses special thanks to John W. Cole for many illuminating discussions pertaining to specific energy requirements for deep space missions. The NASA Principal Investigator was Ron J. Litchford, TD15/ASTP.

.

TRADEMARKS

Available from:

NASA Center for AeroSpace Information
7121 Standard Drive
Hanover, MD 21076–1320
(301) 621–0390

National Technical Information Service
5285 Port Royal Road
Springfield, VA 22161
(703) 487–4650

TABLE OF CONTENTS

LIST OF FIGURES

LIST OF FIGURES (Continued)

LIST OF TABLES

LIST OF ACRONYMS, SYMBOLS, AND ABBREVIATIONS

B	boron
emf	electromotive force
H	hydrogen
He	helium
IMLEO	initial mass in low-Earth orbit
Kr	krypton
Li	lithium
LMD	log-mean difference
MHD	magnetohydrodynamic
MPD	magnetoplasmadynamic
MSNW	Mathematical Sciences Northwest
Nb/Ti	niobium titanium
Nb_3/Sn	niobium tin
NEP	nuclear electric propulsion
NERVA	nuclear engine for rocket vehicle application
STP	standard temperature and pressure
U	uranium
VASIMR	variable specific impulse magneto plasma rocket

NOMENCLATURE

A_c	cross-sectional area
A_{rad}	radiator area
A_{regen}	regenerator area
a	radius of crescent coil half-section
B	magnetic field strength
B_0	centerline magnetic field of single loop
B_c	magnetic field of circular crescent saddle coils
B_H	magnetic field of Helmholtz coils
C_p	specific heat at constant pressure
c	maximum thickness of crescent coil windings
D	diameter
E_r	radial electric field
F	ratio of the radial electrical field strength to the magnetic flux density
G	frictional pressure loss ratio
g_0	gravitational constant
h	mean channel height/enthalpy
h_{ent}	enthalpy at entrance to device
I_{sp}	specific impulse
i	total current
j_c	current density
j_{max}	maximum current density
j_x	current density for the x axis
j_y	current density for the y axis
j_θ	circumferential current density
L	length of the linear generator
M	Mach number
m	mass
$\dot{m}$	mass flow rate
m_c	mass of magnetic coils
m_{comp}	compressor mass
m_{rad}	radiator mass
m_{regen}	regenerator mass

NOMENCLATURE (Continued)

m_{struc}	structural mass
m_{thrust}	thruster mass
N_c	number of compressor stages
n*	relative density
P_0	stagnation pressure
p	pressure
P_{gen}	generator power density
Q_{rad}	radiator thermal power
Q_{reactor}	reactor thermal power
Q_{regen}	regenerator thermal power
$q_{\text{max, regen}}$	theoretical maximum heat transfer for the regenerator
q_{regen}	regenerator heat transfer
$\hat{q}_{\text{rad}}$	radiator specific power per unit specific heat
$\hat{q}_{\text{reactor}}$	reactor specific power per unit specific heat
$\hat{q}_{\text{regen}}$	regenerator specific power per unit specific heat
R	gas constant
R_L	load resistance
r	radius of the disk generator
s_t	material working stress
T	temperature
T_0	stagnation temperature
T_c	compressor stage outlet temperature
$T_{c,s}$	compressor stage outlet temperature for isentropic process
T_e	electron temperature
T_g	bulk gas temperature
T_{max}	maximum operating temperature
T_{min}	minimum operating temperature
u	velocity
U_{regen}	heat transfer coefficient
V	enclosed volume
V_c	volume of magnetic coil winding
V_{gen}	working volume of the generator
W_{comp}	power consumption of the compressor bank
W_e	electrical power

NOMENCLATURE (Continued)

W_{gen}	electrical power output of the generator
W_m	magnetic field energy
W_{thrust}	thruster electrical power
$\hat{w}_{\text{comp}}$	compressor specific power per unit specific heat
$\hat{w}_{\text{gen}}$	generator specific power per unit specific heat
α	specific mass
α_{coil}	specific mass of the coil windings
α_{comp}	specific mass of the compressor
α_{gen}	specific mass of the generator
α_{magnet}	specific mass of the magnet
α_{plant}	specific mass of the nuclear MHD powerplant
α_{rad}	specific mass of the radiator
α_{reactor}	specific mass of the reactor
α_{regen}	specific mass of the regenerator
α_{struc}	specific mass of the reactor
α_{system}	specific mass of the entire propulsion system
α_{thrust}	specific mass of the thruster
β	Hall parameter
β_{rad}	mass per unit area of the radiator
β_{regen}	mass per unit area of the regenerator
γ	specific heat ratio
Δh_{comp}	change of enthalpy across the compressor
$\Delta h_{\text{comp},s}$	isentropic change of enthalpy across the compressor
Δh_{gen}	change in enthalpy within the generator
$\Delta h_{\text{gen},s}$	change in enthalpy for ideal isentropic process
ΔT_a	eq. (49)
ΔT_b	eq. (50)
ΔT_c	compressor temperature rise
ΔT_{LMD}	log-mean temperature difference for the heat exchanger
ε	emissivity
$\varepsilon_{\text{regen}}$	regenerator effectiveness
η_N	enthalpy extraction/addition ratio
η_s	isentropic efficiency
$\eta_{s,c}$	isentropic efficiency of compressor stage

NOMENCLATURE (Continued)

$\eta_{s,g}$	isentropic efficiency of MHD generator
η_t	thruster efficiency
η_{th}	thermal efficiency
μ_0	magnetic permeability
π_c	compression ratio
π_g	pressure ratio across the generator
ρ	material density
ρ_c	magnet material density
σ	bulk electrical conductivity, Stefan-Boltzmann constant
θ	wall angle
ϕ	specific power ($1/\alpha$)

TECHNICAL PUBLICATION

PROSPECTS FOR NUCLEAR ELECTRIC PROPULSION USING CLOSED-CYCLE MAGNETOHYDRODYNAMIC ENERGY CONVERSION

1. INTRODUCTION

From the most fundamental perspective, meaningful scientific and human exploration of deep space will be possible only if there is an abundant source of energy available for propulsion and onboard electrical power production. Furthermore, this energy must be stored in an extremely compact form if it is to be transported along with the spacecraft since any additional mass increment incurs a corresponding increase in energy requirement for orbital transfer. These fundamental considerations place a severe constraint on the minimum acceptable energy density needed for any deep space mission.

To our knowledge, the only plausible means of providing the necessary energy densities, within the context of currently accepted physics, are beamed energy, nuclear energy (fission and fusion), and matter-antimatter annihilation. It should be noted that solar cells may be considered as the onboard conversion component of a beamed energy system with the caveat that the current specific mass for this technology is $\approx$30 kg/kW$_e$ and the perfected value is not expected to fall below 5 kg/kW$_e$. The $1/r^2$ decrease in solar radiation intensity also precludes robust missions beyond Mars.

In principle, any of these energy sources would suffice from the standpoint of energy density alone. However, there are other attributes such as technical maturity, system complexity, energy conversion efficiency, and system specific mass, which stand to differentiate the various technology readiness levels. In terms of these broader system level considerations, nuclear fission space powerplants are the clear standout candidate for near-term realization. This train of thought is by no means unique and can be pursued to certain logical conclusions, as expounded most recently by Sackheim et al.[1]

Given this basic premise, the natural inclination has been toward nuclear-driven, closed-cycle gas turbine installations, since they represent the nearest evolutionary point beyond the existing technology base. Turbogenerator cycles, however, are only effective at low-heat rejection temperatures and as a result require large and massive space radiators. This performance characteristic derives from the fact that practical material limits place severe restrictions on the maximum turbine blade operating temperature, even when the blades are actively cooled, and this, in turn, restricts the maximum cycle temperature. Despite this drawback, these systems have good prospects for approaching a powerplant specific mass below the 10-kg/kW$_e$ mark.

The major culprit affecting heat engine weight is the space radiator. Because the specific mass of the radiator is proportional to $1/T^4$, the radiator weight can greatly exceed the reactor and energy conversion component weights when forced to operate at a low-heat rejection temperature. Therefore, there is a strong incentive to break through the 1-kg/kW$_e$ barrier by finding an alternative means of elevating the

cycle operating temperature and thereby increasing the heat rejection temperature. The natural alternative for attaining this goal is magnetohydrodynamic (MHD) energy conversion.

The primary reason for considering MHD is the ability to extract energy from a flowing gas at arbitrarily high temperatures. As such, an MHD converter can operate effectively at temperatures beyond the realm of actively cooled turbine blade technology. Using demonstrated solid core and fixed particle bed reactor technology, for example, it is possible to push peak operating temperatures to 2,500 K with minimum development risk, and this value could readily be raised to 3,000 K with further development of advanced high-temperature fissile fuels, particularly ternary carbide elements. Even operating temperatures beyond 3,000 K are conceivable with the introduction of gas core reactors in which the fissile fuel is allowed to circulate throughout the power conversion system. The useful upper limit for gas core reactors with MHD energy conversion is estimated to be as high as 8,000–10,000 K, at which point the rapid increase in free electron radiation makes regenerative cooling extremely difficult as well as causing the gas cooling timescale to fall—most likely below the channel residence timescale.

The most common configurations for MHD generators are the (a) linear channel and the (b) radial disk, as illustrated in figure 1. In either case, an external magnetic field, B, is imposed perpendicular to the flow path and the motion of the electrically conductive gas interacts with the magnetic field to develop a Faraday electromotive force (emf) orthogonal to both the flow velocity and the magnetic field and a Hall emf directed along the flow path. The value of the Hall emf relative to the Faraday emf depends upon the value of the Hall parameter, β. When β is on the order of unity or greater, the Hall configured disk geometry is used predominately since it avoids the complicated electrode segmentation requirements associated with the design of linear channels.

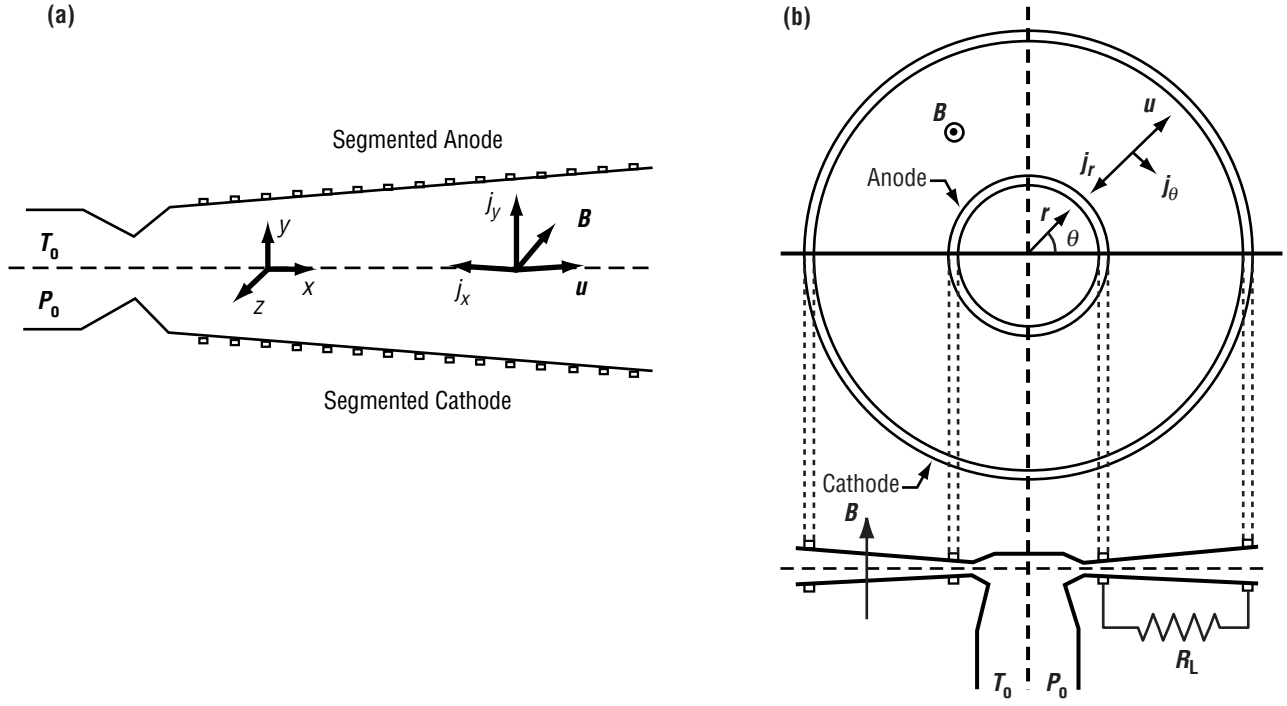

Figure 1. Schematics of (a) linear and (b) disk MHD generator configurations.

The induced Faraday and Hall emf's result in a current flow in the gas, which is transferred to an external load through contact electrodes in the channel. The interaction of the current with the magnetic field produces a retarding force on the gas, thereby forcing it to do push work as it moves through the generator channel. Therefore, there is a pressure drop across the MHD converter in direct analogy to that experienced by a turbine stage. The difference being that the stationary and lightly stressed MHD channel walls can be cooled to temperatures much lower than the core gas temperature in the same manner that the chamber walls of a chemical rocket engine are regeneratively cooled. In this case, it is the heat transfer rate, not the core gas temperature, that determines engineering feasibility.

Nuclear MHD space power systems, as summarized above, were first conceived and conceptually developed by R.J. Rosa in the 1960's.[2–8] Since then, the idea has been periodically revived and amplified in relation to various perceived space power needs.[9–15] Yet, this technology has never progressed beyond studies and low-priority research efforts, despite its many positive attributes. And it remains to this day, a potentially high payoff concept for which the perceived risk far exceeds the actual development risk.

This Technical Publication revives the concept once more and amplifies on the scenario for a nuclear MHD space powerplant coupled with high-power electric thrusters. The emphasis here is to demonstrate that these systems could immensely broaden deep space mission capability while adhering to a technology development path that is entirely within established bounds of engineering feasibility. These conclusions are obtained through a preliminary but thorough system analysis in which the various component characteristics are estimated using established data or, when an empirical database is unavailable, using widely accepted extrapolations from current state-of-the-art technology. Additional technological development opportunities are also examined in terms of potential payoff versus development risk.

2. SYSTEM ANALYSIS

Generally speaking, high-power density fission reactors are adaptable to both Brayton and Rankine energy conversion cycles. For example, Rankine cycles, by taking advantage of the gas-to-liquid phase transition, provide superior performance for a fixed overall temperature differential, and they can completely avoid the limitations of compressor turbomachinery. Unfortunately, the condensing vapors tend to be highly corrosive, raising significant design and reliability concerns. Brayton cycles, on the other hand, are simpler, exhibit only slightly inferior performance, and promise increased reliability in that they are more suited for utilization of an inert gas working fluid.

Although previous studies have established the fact that Rankine MHD cycles can provide substantially lower system specific mass,[2–8,11,12] the authors take the point of view that Brayton MHD cycles are more directly compatible with solid-core, gas-cooled reactors and can more effectively leverage the existing technology base. Therefore, they appear to offer a lower risk development path in the near term while maintaining a significant payoff in comparison to turbogenerator systems. As such, the Brayton MHD cycle with regenerative heating and intercooled multistage compression forms the focus of attention for further investigation.

The essential components of a nuclear electric propelled spacecraft based on a closed-loop MHD Brayton cycle are shown in figure 2. From the perspective of mass distribution, it is useful to lump the spacecraft subsystems into three categories: the payload, the propellant, and the thrust producing system. The major thrust of this work was to analyze the specific mass characteristics of the powerplant and the integrated propulsion system and to make a status/risk assessment of the various enabling technologies. Since the powerplant is the dominant contributor to overall spacecraft weight, there is intense interest in obtaining accurate estimates of powerplant specific mass characteristics as a means of delineating technological capabilities and limitations. Once the specific mass characteristics are quantitatively defined to a satisfactory degree of accuracy, it becomes possible to comparatively assess various technological approaches and to identify the major technology development challenges and associated risks.

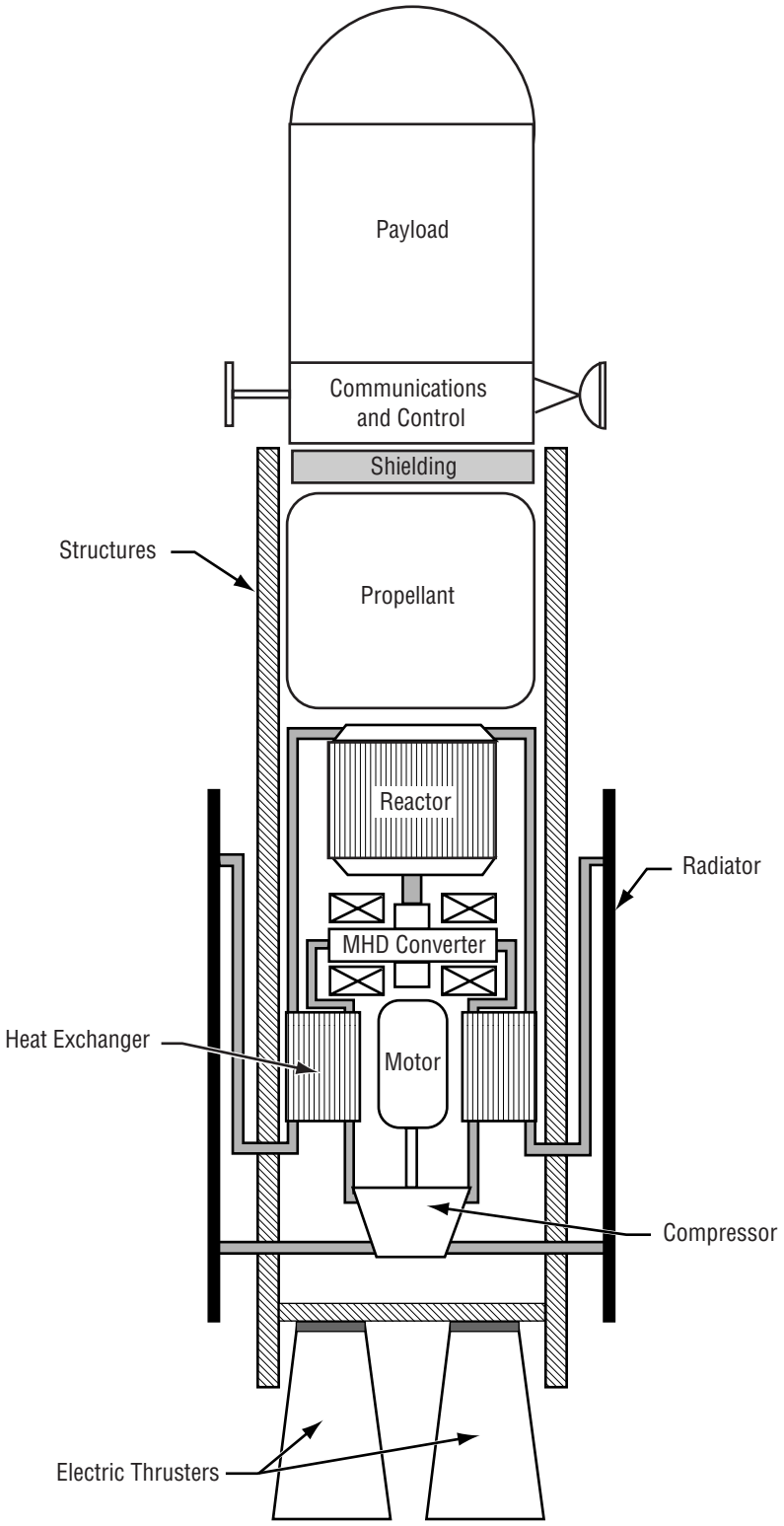

Figure 2. Essential components of a nuclear electrical propelled spacecraft based on a closed-loop MHD Brayton cycle powerplant.

For reference purposes, a schematic of a closed-loop nuclear MHD Brayton cycle powerplant coupled to high-power electric propulsion is provided in figure 3. The temperature-entropy diagram for the closed-loop Brayton power cycle is also shown in figure 4. The thermodynamic cycle is now analyzed assuming fixed maximum (T_{max}) and minimum (T_{min}) operating temperatures.

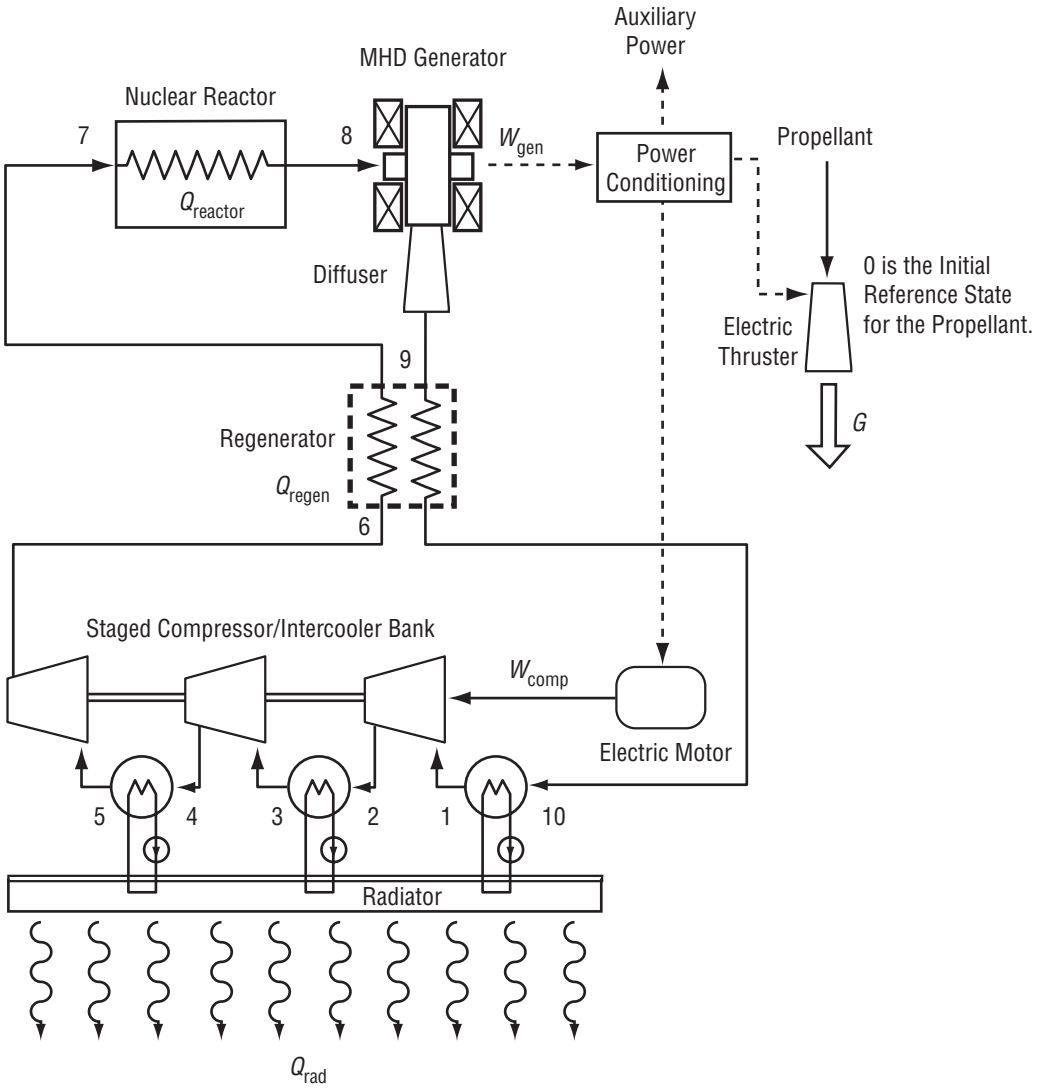

Figure 3. Schematic of a closed-loop nuclear MHD Brayton cycle powerplant with regenerative heating and intercooled multistage compression. Installation is shown coupled to high-power electric propulsion.

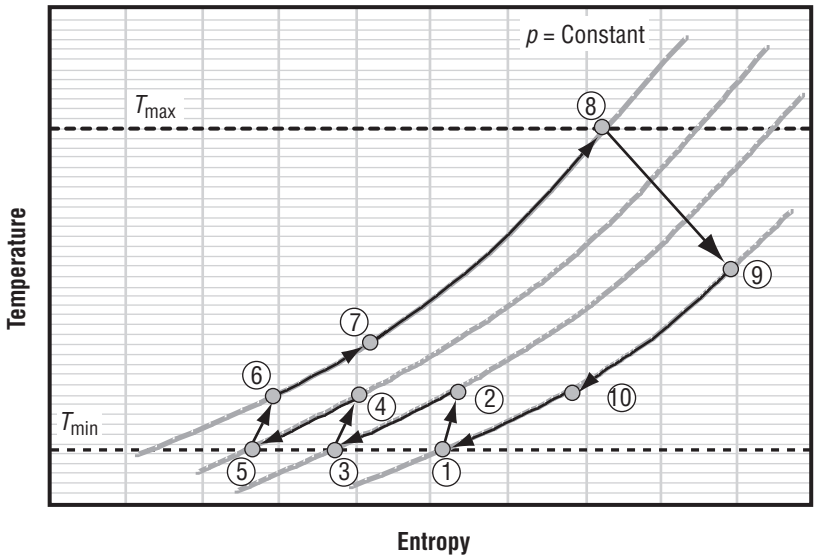

Figure 4. Temperature-entropy diagram for a closed-loop Brayton cycle powerplant with regenerative heating and intercooled multistage compression.

2.1 Thermodynamic Cycle Analysis

In the special case where all net power production is used for propulsion, the thermal efficiency (η_{th}) of the powerplant is equivalent to the ratio of thruster electric power (W_{thruster}) to reactor thermal power (Q_{reactor}):

$$\eta_{\text{th}} = \frac{W_{\text{thruster}}}{Q_{\text{reactor}}} = \frac{W_{\text{gen}} - W_{\text{comp}}}{Q_{\text{reactor}}} \cong \frac{\left(T_{\max} - T_9\right) - N_c\left(T_2 - T_{\min}\right)}{T_{\max} - T_7} \quad , \tag{1}$$

where W_{gen} is the electrical power output of the generator, W_{comp} is the power consumption of the compressor bank, and N_c is the number of compressor stages. In addition, it is assumed $T_{\min} = T_1 = T_3 = T_5 \ldots$ is the effective radiator temperature.

In analyzing the MHD generator, it is useful to note that any MHD device can be described in terms of two fundamental process parameters: an enthalpy extraction/addition ratio (η_N) and an isentropic efficiency (η_s) which quantifies the degree of departure from an isentropic process.

The enthalpy extraction parameter for the generator is defined as the ratio of the change in enthalpy Δh_{gen} to the entrance enthalpy h_{ent}:

$$\eta_N = \frac{\Delta h_{\text{gen}}}{h_{\text{ent}}} = \frac{h_8 - h_9}{h_8} \cong \frac{T_{\max} - T_9}{T_{\max}} \tag{2}$$

or

$$T_9 = \left(1 - \eta_N\right) T_{\max} \quad . \tag{3}$$

For an MHD generator (enthalpy extraction), the isentropic efficiency $\eta_{s,g}$ is defined as the ratio of the actual change in enthalpy to that for an ideal isentropic process $\Delta h_{\text{gen},s}$:

$$\eta_{s,g} = \frac{\Delta h_{\text{gen}}}{\Delta h_{\text{gen},s}} = \frac{h_8 - h_9}{h_8 - h_{9,s}} \cong \frac{T_{\max} - T_9}{T_{\max} - T_{9,s}} \tag{4}$$

or

$$T_9 = \left\{1 - \eta_{s,g}\left[1 - \frac{T_{9,s}}{T_{\max}}\right]\right\} T_{\max} \quad . \tag{5}$$

Using the isentropic process relationship for an ideal gas, it is possible to write equation (5) in the form:

$$T_9 = \left\{1 - \eta_{s,g}\left[1 - \pi_g^{-\frac{\gamma-1}{\gamma}}\right]\right\} T_{\max} \quad , \tag{6}$$

where $\pi_g = p_8 / p_9$ is the pressure ratio across the generator and γ is the specific heat ratio. Combining equations (3) and (6) yields a fundamental relationship between η_N and $\eta_{s,g}$:

$$\eta_N = \eta_{s,g}\left[1 - \pi_g^{-\frac{\gamma-1}{\gamma}}\right] \quad . \tag{7}$$

The N_c compressor stages are assumed to operate with the same temperature rise $\Delta T_c = T_c - T_{\min}$ such that $T_c = T_2 = T_4 = T_6 \ldots$ Furthermore, in order to compensate for the net pressure drop in the system, the pressure ratio across the MHD generator is defined as $\pi_g = G\pi_c^{N_c}$ such that each compressor stage has a common compression ratio (π_c):

$$\pi_c = \left(\frac{\pi_g}{G}\right)^{1/N_c} = \frac{p_2}{p_1} = \frac{p_4}{p_3} = \frac{p_6}{p_5} \quad \ldots \tag{8}$$

The parameter G represents a pressure loss ratio due to frictional losses ($0 < G \leq 1$). Thus, for each compressor stage (enthalpy addition), the isentropic efficiency ($\eta_{s,c}$) is defined as

$$\eta_{s,c} = \frac{\Delta h_{\text{comp},s}}{\Delta h_{\text{comp}}} = \frac{h_{c,s} - h_{\min}}{h_c - h_{\min}} \cong \frac{T_{c,s} - T_{\min}}{T_c - T_{\min}} \quad , \tag{9}$$

which can be reformulated in terms of T_c:

$$T_C = \left\{1 + \frac{1}{\eta_{s,c}}\left[\frac{T_{c,s}}{T_{\min}} - 1\right]\right\} T_{\min} \quad . \tag{10}$$

By using the isentropic process relationship for an ideal gas and using equation (8) to eliminate π_c, it is possible to write equation (10) in the form:

$$T_c = T_2 = T_4 = T_6 = \left\{1 + \frac{1}{\eta_{s,c}}\left[\left(\frac{\pi_g}{G}\right)^{\frac{\gamma-1}{\gamma N_c}} - 1\right]\right\} T_{\min} \quad . \tag{11}$$

Regenerative heating is employed in the cycle to increase thermal efficiency and reduce the amount of waste heat that must be rejected by the radiator. The regenerator effectiveness is defined as

$$\varepsilon_{\text{regen}} = \left.\frac{q}{q_{\max}}\right|_{\text{regen}} = \frac{h_7 - h_6}{h_9 - h_6} \cong \frac{T_7 - T_6}{T_9 - T_6} \quad , \tag{12}$$

which yields

$$T_7 = \varepsilon_{\text{regen}}\left(T_9 - T_6\right) + T_6 \tag{13}$$

or, upon substitution of equations (6), (7), and (11),

$$T_7 = \varepsilon_{\text{regen}}\left(1 - \eta_N\right) T_{\max} + \left(1 - \varepsilon_{\text{regen}}\right)\left\{1 + \frac{1}{\eta_{s,c}}\left[\left(\frac{\pi_g}{G}\right)^{\frac{\gamma-1}{\gamma N_c}} - 1\right]\right\} T_{\min} \quad . \tag{14}$$

A power balance on the regenerator requires that

$$\frac{h_9 - h_{10}}{h_7 - h_6} = \frac{T_9 - T_{10}}{T_7 - T_6} = 1 \tag{15}$$

or

$$T_{10} = T_9 - \left(T_7 - T_6\right) \ . \tag{16}$$

Thus, equations (13) and (16) may be combined to obtain the form:

$$T_{10} = \left(1 - \varepsilon_{\text{regen}}\right) T_9 - \varepsilon_{\text{regen}} T_6 \ . \tag{17}$$

Then, substitution for T_9 and T_6 using equations (6), (7), and (11) gives an expression for T_{10} in terms of the cycle operating temperatures and process parameters:

$$T_{10} = \left(1 - \varepsilon_{\text{regen}}\right)\left\{1 - \eta_N\right\} T_{\max} + \varepsilon_{\text{regen}} \left\{1 + \frac{1}{\eta_{s,c}} \left[\left(\frac{\pi_g}{G} \right)^{\frac{\gamma - 1}{\gamma N_c}} - 1 \right] \right\} T_{\min} \ . \tag{18}$$

The various thermodynamic states throughout the cycle have now been expressed in terms of the reactor and radiator operating temperatures and the various component process parameters. This information may further be used to deduce the power per unit mass flow per unit specific heat for each system component. The results are summarized as follows:

$$\hat{q}_{\text{reactor}} = \frac{Q_{\text{reactor}}}{\dot{m} C_p} = \left\{1 - \varepsilon_{\text{regen}}\left[1 - \eta_N\right]\right\} T_{\max} - \left(1 - \varepsilon_{\text{regen}}\right) \left\{1 + \frac{1}{\eta_{s,c}} \left[\left(\frac{\pi_g}{G} \right)^{\frac{\gamma - 1}{\gamma N_c}} - 1 \right] \right\} T_{\min} \ , \tag{19}$$

$$\hat{w}_{\text{gen}} = \frac{W_{\text{gen}}}{\dot{m} C_p} = \eta_N T_{\max} \ , \tag{20}$$

$$\hat{w}_{\text{comp}} = \frac{W_{\text{comp}}}{\dot{m} C_p} = \frac{N_c}{\eta_{s,c}} \left[\left(\frac{\pi_g}{G} \right)^{\frac{\gamma - 1}{\gamma N_c}} - 1 \right] T_{\min} \ , \tag{21}$$

$$\hat{q}_{\text{regen}} = \frac{Q_{\text{regen}}}{\dot{m} C_p} = \varepsilon_{\text{regen}} \left(1 - \eta_N\right) T_{\max} - \varepsilon_{\text{regen}} \left\{1 + \frac{1}{\eta_{s,c}} \left[\left(\frac{\pi_g}{G} \right)^{\frac{\gamma - 1}{\gamma N_c}} - 1 \right] \right\} T_{\min} \ , \tag{22}$$

and

$$\hat{q}_{\text{rad}} = \frac{Q_{\text{rad}}}{\dot{m}C_p} = \left(1-\varepsilon_{\text{regen}}\right)\left(1-\eta_N\right)T_{\max} - \left(1-\varepsilon_{\text{regen}}\right)\left\{1+\frac{1}{\eta_{s,c}}\left[\left(\frac{\pi_g}{G}\right)^{\frac{\gamma-1}{\gamma N_c}}-1\right]\right\}T_{\min}$$

$$-\frac{C_p\left(N_c-1\right)}{\eta_{s,c}}\left[\left(\frac{\pi_g}{G}\right)^{\frac{\gamma-1}{\gamma N_c}}-1\right]T_{\min} \ . \tag{23}$$

It is also possible to frame the cycle thermal efficiency in similar terms by substituting equations (19)–(21) into equation (1):

$$\eta_{\text{th}} = \frac{\eta_{s,g}\left[1-\pi_g^{-\frac{\gamma-1}{\gamma}}\right]T_{\max} - \frac{N_c}{\eta_{s,c}}\left[\left(\frac{\pi_g}{G}\right)^{\frac{\gamma-1}{\gamma N_c}}-1\right]T_{\min}}{\left[1-\varepsilon_{\text{regen}}\left\{1-\eta_{s,g}\left[1-\pi_g^{-\frac{\gamma-1}{\gamma}}\right]\right\}\right]T_{\max} - \left(1-\varepsilon_{\text{regen}}\right)\left\{1+\frac{1}{\eta_{s,c}}\left[\left(\frac{\pi_g}{G}\right)^{\frac{\gamma-1}{\gamma N_c}}-1\right]\right\}T_{\min}} \ . \tag{24}$$

2.2 Specific Mass Analysis

Thermal efficiency is not the central consideration for space installations. Rather, the entire system must be examined in terms of its overall mass relative to its performance. This requires a careful evaluation of all subcomponent mass characteristics in order to obtain an estimate of the aggregate system mass.

The aggregate specific mass of the nuclear MHD powerplant is defined as

$$\alpha_{\text{plant}} = \frac{\alpha\hat{q}\big|_{\text{reactor}} + \alpha\hat{w}\big|_{\text{gen}} + \alpha\hat{w}\big|_{\text{comp}} + \alpha\hat{q}\big|_{\text{regen}} + \alpha\hat{q}\big|_{\text{rad}}}{\hat{w}_{\text{gen}} - \hat{w}_{\text{comp}}} \ . \tag{25}$$

The specific mass of the combined powerplant and electric thruster, which is assumed here to include all necessary power conditioning equipment, is therefore given by

$$\alpha_{\text{system}} = \alpha_{\text{plant}} + \alpha_{\text{thrust}} \ . \tag{26}$$

It is also common practice to define the specific power as $\phi = 1/\alpha$. Specification of the subcomponent specific mass characteristics now follows.

2.2.1 Fission Reactor

Ample experience indicates that solid core and fixed particle bed reactors can provide peak temperatures in the 2,500–3,000 K range. The solid-core nuclear engine for rocket vehicle application (NERVA) engine, for instance, had a design operating temperature of 2,500 K, and a low-risk development path was identified for increasing this limit to 3,000 K through the development of high-temperature carbide fuels.[16] As such, this technology base can be used to estimate anticipated reactor specific mass. Using the NERVA technology as an empirical basis, for instance, Holman has developed a 350 MW_{th} reactor design having a mass of 1,785 kg. This yields a specific power of 0.2 MW_{th}/kg.

Within reasonable bounds, the reactor mass can be assumed independent of reactor power level, and the authors conservatively estimate a reactor mass of 3,000 kg, which includes margin for shielding. Thus,

$$\alpha_{\text{reactor}} = \frac{m_{\text{reactor}}}{Q_{\text{reactor}}} = \frac{3{,}000 \text{ kg}}{Q_{\text{reactor}}} \quad . \tag{27}$$

2.2.2 Magnetohydrodynamic Generator

There are strong incentives to operate MHD devices at very high magnetic flux densities. For example, the power density of an ideal MHD generator varies as $\sigma u^2 B^2$, where σ is the bulk electrical conductivity, u is the velocity, and B is the magnetic field strength. Since σ and u have practical limitations, it is therefore desirable to have B as large as practically feasible. Furthermore, Hall-configured disk generators can exhibit high isentropic efficiency only when the Hall parameter is large ($\beta > 10$).[17] Again, high magnetic flux densities are required since $\beta \propto B/p$, where p is the static pressure in the device.

Because of this basic need for large values of B, the weight of the generator as a whole is dominated almost exclusively by the weight of the magnet. The magnet weight, in turn, is determined mainly by the weight of the confinement structure and the weight of the coils. Under these assumptions, the generator specific mass is defined by

$$\alpha_{\text{gen}} \approx \alpha_{\text{magnet}} = \alpha_{\text{struc}} + \alpha_{\text{coil}} \quad , \tag{28}$$

where α_{magnet} is the specific mass of the magnet, α_{struc} is the specific mass of the structure, and α_{coil} is the specific mass of the coil windings.

It is not practical to entertain the utilization of dissipative magnets in space installations, mainly due to the excessive weight penalties associated with waste heat rejection. Therefore, only supergenic (i.e., superconducting-cryogenic type coils) are considered in which a high field superconductor (e.g., Nb_3/Sn or Nb/Ti) is embedded in a metal base material (i.e., copper or aluminum) as a means of providing quench stabilization. It is also assumed that flux pumping techniques will be utilized in order to minimize the auxiliary equipment needed for magnet power-up.

2.2.3 Magnet Confinement Structure

The basic challenge of large-volume, high-field magnet design can be readily summarized. Because magnetic flux density falls off with distance from the coil as $1/r^2$, very large currents are necessary to fill the working volume, and this, in turn, leads to the exertion of extremely large Lorentz forces on the coil. Therefore, a large confinement structure is needed to support those forces that the conducting coils cannot withstand themselves.

The confinement requirements may be fundamentally expressed in terms of the stored magnetic field energy, W_m:

$$W_m = \iiint_V \frac{B^2}{2\mu_0}\, dV \cong \frac{B^2}{2\mu_0} V \quad , \tag{29}$$

where μ_0 is the magnetic permeability and V is the enclosed volume. The Virial theorem may then be used as an estimate of the minimal mass due to structural requirements (i.e., ideal hoop tension to contain the stored energy):

$$m_{\text{struc}} \geq \frac{\rho}{s_t} W_m \cong \frac{\rho}{s_t} \frac{B^2}{2\mu_0} V \quad , \tag{30}$$

where ρ is the material density and s_t is the material working stress. Some typical values for $W_m/m = s_t/\rho$ are summarized in table 1.

Table 1. Virial theorem requirements.

Material	$W_m/m = s_t/\rho$ (kJ/kg)
Fiber-reinforced composites	10–50
Stainless steel (304LN)	44
Aluminum (2219T851)	107
Titanium	309
Beryllium-Copper	580

At this point, it is convenient to introduce the generator power density, $P_{\text{gen}} = W_{\text{gen}}/V$, into equation (30) to arrive at a working specific mass estimate for the confinement structure:

$$\alpha_{\text{struc}} = \frac{m_{\text{struc}}}{W_{\text{gen}}} = \frac{\rho}{s_t} \frac{B^2/2\mu_0}{P_{\text{gen}}} \quad . \tag{31}$$

2.2.4 Saddle Coil Winding—Linear Generator

Consider the coil requirements for a linear generator channel. Based on conservative design experience, assume a minimal channel aspect ratio of $L/D = 10$. This ratio is recommended by Rosa in order to minimize nonideal losses associated with large surface-to-volume effects.[18] In this case, the working volume of the generator can be expressed as

$$V_{\text{gen}} = \frac{W_{\text{gen}}}{P_{\text{gen}}} = \frac{\pi}{4} D^2 L = \frac{5\pi}{2} D^3 \quad , \tag{32}$$

which yields a nominal generator diameter of

$$D = \left(\frac{2}{5\pi} \frac{W_{\text{gen}}}{P_{\text{gen}}} \right)^{\frac{1}{3}} \quad . \tag{33}$$

A uniform magnetic field can be produced within the generator volume if the saddle coil windings approximate a circular crescent cross section of diameter D, as illustrated in figure 5. The total cross-sectional area (A_c) of the winding on each side is

$$A_c \approx 2ca = 2c\left(\frac{D}{2} + \frac{c}{2} \right) = c(c + D) = cD\left(\frac{c}{D} + 1 \right) \quad . \tag{34}$$

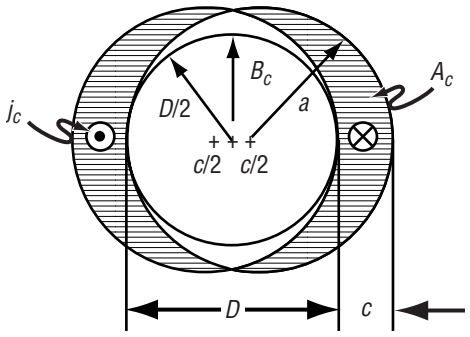

Figure 5. Illustration of a circular crescent coil cross section for a linear channel of diameter D. Note that $2a = D + c$ is a geometric constraint.

In the limit $c/D \rightarrow 0$, $A_c \approx cD$ and a uniform constant magnetic field (B_c) is produced which is defined by

$$B_c = \frac{B_0}{2} = \frac{\mu_0 i}{4r} = \frac{\mu_0 j_c A_c}{2D} = \frac{\mu_0 j_c c}{2} \quad , \tag{35}$$

where i is the total current, j_c is the current density, and $B_0 = \mu_0 i/2r$ is the field produced in a loop of diameter $D = 2r$. The value for j_c can be as high as 10^9 A/m^2 for Nb_3/Sn-based superconductors.

Using equations (33) and (35) to eliminate D and c in equation (34) gives an expression for the cross-sectional area in terms of the material properties, the generator power characteristics, and the required magnetic flux density:

$$A_c = \frac{2B_c}{\mu_0 j_c}\left[\frac{2B_c}{\mu_0 j_c} + \left(\frac{2}{5\pi}\frac{W_{\text{gen}}}{P_{\text{gen}}}\right)^{\frac{1}{3}}\right] . \tag{36}$$

The mass of the magnet coils may now be deduced from the relation:

$$m_c = \rho_c V_c = 2\rho_c A_c L = 20\rho_c A_c D \tag{37}$$

and the specific mass of the coil windings takes the form:

$$\alpha_{\text{coil}} = \frac{m_c}{W_{\text{gen}}} = \frac{20\rho_c A_c D}{W_{\text{gen}}} , \tag{38}$$

where D is defined by equation (33).

2.2.5 Helmholtz Coil Winding—Disk Generator

Consider the coil requirements for an MHD disk generator of radius r and mean channel height h. Based on conservative design experience, assume a minimal channel aspect ratio of $r/h = 10$ in analogy to the length-to-diameter ratio assumed for the linear configuration. Again, this value is recommended by Rosa in order to minimize nonideal losses associated with large surface-to-volume effects.[18] Thus, $D/h = 20$, and the working volume of the generator can be expressed as

$$V_{\text{gen}} = \frac{W_{\text{gen}}}{P_{\text{gen}}} = \frac{\pi}{4}D^2 h = \frac{\pi}{80}D^3 . \tag{39}$$

This yields a nominal disk diameter of

$$D = \left(\frac{80}{\pi}\frac{W_{\text{gen}}}{P_{\text{gen}}}\right)^{\frac{1}{3}} . \tag{40}$$

Helmholtz coil windings of diameter D, as illustrated in figure 6, can then be used to produce a uniform magnetic field B_H within the disk volume:

$$B_H = \frac{B_0}{\sqrt{2}} = \frac{\mu_0 i}{2\sqrt{2}r} = \frac{\mu_0 j_c A_c}{\sqrt{2}D} \quad . \tag{41}$$

This expression can be combined with equation (40) to arrive at an expression for the cross-sectional area of the winding in terms of the material properties, the generator power density, and the required magnetic flux density:

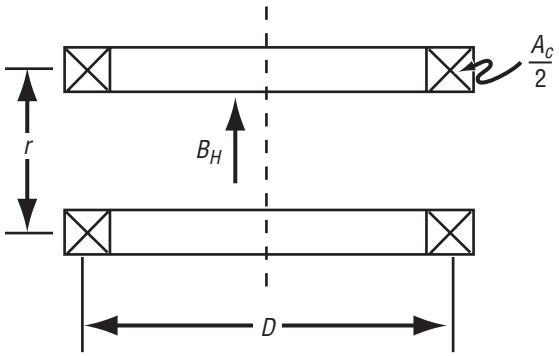

Figure 6. Illustration of a Helmholtz coil winding for a disk generator of diameter D. Note that the coils are separated by a distance $r = D/2$.

$$A_c = \frac{\sqrt{2}B_H}{\mu_0 j_c}\left(\frac{80}{\pi}\frac{W_{\text{gen}}}{P_{\text{gen}}}\right)^{\frac{1}{3}} \quad . \tag{42}$$

The mass of the magnet coils may now be deduced from the relation:

$$m_c = \rho_c V_c = \rho_c \pi D A_c = \frac{\sqrt{2}\pi\rho_c B_H D^2}{\mu_0 j_c} \tag{43}$$

and the specific mass of the coil windings takes the form:

$$\alpha_{\text{coil}} = \frac{m_c}{W_{\text{gen}}} = \frac{\sqrt{2}\pi\rho_c B_H D^2}{\mu_0 j_c W_{\text{gen}}} \quad , \tag{44}$$

where D is defined by equation (40).

2.2.6 Turbocompressors

The weight characteristics of the turbocompressors and drive can be accurately estimated from a broad body of technical experience. Following Rosa, it is assumed that the specific mass of the compressor group is given by

$$\alpha_{\text{comp}} = \frac{m_{\text{comp}}}{W_{\text{comp}}} = 2 \times 10^{-5} \text{ kg/W} \quad . \tag{45}$$

2.2.7 Regenerator

The regenerator is assumed to be a typical compact shell and tube heat exchanger for which the specific mass attributes can be estimated accurately. A conservative value for the mass per unit area of this type of heat exchanger is

$$\beta_{\text{regen}} = \frac{m_{\text{regen}}}{A_{\text{regen}}} = 1 \text{ kg/m}^2 \quad . \tag{46}$$

Assuming a constant value for the overall heat transfer coefficient, U_{regen}, it is possible to express the total heat transfer rate in the form:

$$Q_{\text{regen}} = U_{\text{regen}} \Delta T_{\text{LMD}} A_{\text{regen}} \quad , \tag{47}$$

where ΔT_{LMD} is the log-mean temperature difference for the heat exchanger and is defined as

$$\Delta T_{\text{LMD}} = \frac{\Delta T_b - \Delta T_a}{\ln\left(\frac{\Delta T_b}{\Delta T_a}\right)} \quad , \tag{48}$$

and

$$\Delta T_a = T_{\text{hot,in}} - T_{\text{cold,out}} \quad , \tag{49}$$

$$\Delta T_b = T_{\text{hot,out}} - T_{\text{cold,in}} \quad . \tag{50}$$

In the limit $\left| \Delta T_b / \Delta T_a \right| \to 1$,

$$\lim_{\left|\frac{\Delta T_b}{\Delta T_a}\right| \to 1} \Delta T_{\text{LMD}} = \frac{\Delta T_b + \Delta T_a}{2} \quad . \tag{51}$$

Note that the temperatures used to calculate ΔT_{LMD} are obtained from the thermodynamic cycle analysis based on an assumed value for the regenerator effectiveness.

If equations (46) and (47) are now combined to eliminate A_c, the specific mass of the regenerator takes the form:

$$\alpha_{\mathrm{regen}} = \frac{m_{\mathrm{regen}}}{Q_{\mathrm{regen}}} = \frac{\beta_{\mathrm{regen}}}{U_{\mathrm{regen}} \Delta T_{\mathrm{LMD}}} \quad . \tag{52}$$

2.2.8 Radiator

Space radiators tend to dominate the weight of multimegawatt heat engine installations, and nuclear-electric propulsion systems can quickly become impractical due to the impact on overall system specific mass. Issues of reliability and survivability also escalate with increasing size. The important design parameter for space radiators is the mass per unit area defined as

$$\beta_{\mathrm{rad}} = \frac{m_{\mathrm{rad}}}{A_{\mathrm{rad}}} \approx 1 - 0.2 \ \mathrm{kg/m^2} \ . \tag{53}$$

The upper range for β_{rad} represents projected estimates for conventional radiator design whereas the lower range for β_{rad} corresponds to projections for liquid droplet radiator concepts.

The radiative power is given by

$$Q_{\mathrm{rad}} = \varepsilon \sigma A_{\mathrm{rad}} T_{\mathrm{min}}^4 \ , \tag{54}$$

where ε is the emissivity and σ is the Stefan-Boltzmann constant. If equations (53) and (54) are combined to eliminate A_{rad}, the specific mass of the radiator takes the form:

$$\alpha_{\mathrm{rad}} = \frac{m_{\mathrm{rad}}}{Q_{\mathrm{rad}}} = \frac{\beta_{\mathrm{rad}}}{\varepsilon \sigma T_{\mathrm{min}}^4} \quad . \tag{55}$$

2.2.9 Electric Thruster

Many nuclear-electric deep space transport missions exhibit optimal results for an idealized thruster having a specific impulse in the range of 2,500 to 1,500 sec and a thrust in the range of 10 to 1,000 N. For a thruster efficiency $\eta_t = 50\%$, the fundamental equation of electric propulsion would imply a nominal power range of

$$W_e = F\frac{g_0 I_{sp}}{2\eta_t} \approx 0.25 - 15 \ \ \mathrm{MW_e} \ , \tag{56}$$

where F is the thrust, I_{sp} is the specific impulse, and g_0 is the Earth's gravitational constant.

In reality, efficient, high-thrust electric propulsion has yet to be demonstrated, and the prevalent opinion among specialists is that electric thrusters can only be effective at low thrust levels. Nevertheless, there is some hope that certain electric thruster devices may be scaleable to multimegawatt power levels and yet remain compact and reliable. The variable specific impulse magneto plasma rocket (VASIMR) concept even holds the promise of constant power throttling which allows both thrust and specific impulse to be continuously varied.[19] Extensive calculations by Slavin et al. also indicate that an MHD high-temperature current- (T-) layer type of engine using neon propellant could potentially produce 1,000 N of thrust at a specific impulse of 2,000 sec with an electrical efficiency of more than 90%.[15]

Some representative electric thruster characteristics, including conservative estimates for specific mass, are summarized in table 2. Note that these are only approximate figures of merit based on a broad body of technical experience. Here, the specific mass is defined in terms of the plant electrical power delivered to the thruster:

$$\alpha_{\mathrm{thrust}} = \frac{m_{\mathrm{thrust}}}{W_{\mathrm{thrust}}} = \frac{m_{\mathrm{thrust}}}{W_{\mathrm{gen}} - W_{\mathrm{comp}}} \ . \tag{57}$$

Table 2. Electric thruster characteristics.*

Device	I_{sp} (sec)	η_t	α (kg/kW$_e$)
Ion (Kr)	≥5,000	0.8	1.0
MPD (Li)	4,000–8,000	0.5	0.5
MPD (H_2)	≥8,000	0.5	0.5
VASIMR (H_2)	3,000–30,000	0.5	0.2–1.0

*Approximated values

3. SYSTEM ASSESSMENT

Based on the preceding development, representative system analysis calculations were performed as a means of assessing system attributes. First, thermodynamic cycle characteristics were investigated over a practical range of $T_{\min}$ and π_g; i.e., η_N, parameter space. The assumed system characteristics, based on established bounds of engineering capability, are as follows: Helium working fluid, $T_{\max}$ = 2,500 K, $\varepsilon_{\text{regen}} = 0.9$, $\eta_{s,g} = 70\%$, and $\eta_{s,c} = 87\%$. All calculations were performed assuming no frictional pressure losses (i.e., G=1).

The resulting thermal efficiency contour map for the MHD Brayton cycle is shown in figure 7. Note that the peak cycle efficiency moves to larger pressure ratios as the minimum cycle temperature falls. The highest achievable thermal efficiency approaches 70% as the heat rejection temperature approaches 200 K. For space applications, however, thermal efficiency is secondary in importance to system specific mass.

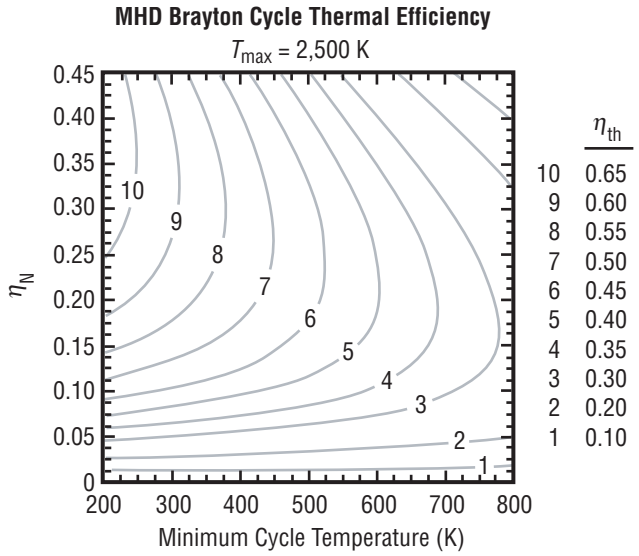

Figure 7. Thermal efficiency of an MHD generator Brayton cycle using helium as the working fluid.

For demonstration purposes, the authors assumed a reactor power of W_{gen} = 100 MW_{th} and explored the specific mass characteristics over a similar range of $T_{\min}$ and π_g (i.e., η_N), parameter space. Two sets of subsystem technology assumptions were investigated. These assumptions were based on conservative estimates of near-term and advanced subsystem technologies, as summarized in table 3. The major anticipated technology advances are as follows: An increase in s_t/ρ through utilization of beryllium-copper material for the magnet structure, a decrease in ρ_c through utilization of aluminum as the base material for the supergenic coil, major reduction in radiator specific mass through the introduction of liquid droplet technology, and slight evolutionary improvements in thruster efficiency and specific mass.

Table 3. Subsystem technology assumptions.

Parameter	Near Term	Advanced
$m_{reactor}$ (kg)	3,000	3,000
P_{gen} (MW_e/m^3)	500	500
B (tesla)	8	8
σ/s_t (kJ/kg)	309	580
ρ_c (kg/m^3)	1×10^4	3×10^3
j_c (A/m^2)	1×10^9	1×10^9
U_{regen} (W/m^2 K)	500	500
β_{regen} (kg/m^2)	1	1
ε_{rad}	0.9	0.9
β_{rad} (kg/m^2)	1	0.2
η_{thrust} (%)	50	60
α_{thrust} (kg/kW_e)	0.5	0.4

The resulting contour maps for the disk MHD powerplant specific mass are given in figure 8. For the near-term technology assumptions, it is found that the powerplant specific mass can be less than 0.4 kg/kW_e at a heat rejection temperature of ≈700 K and an enthalpy extraction ratio of ≈20%. For the advanced technology assumptions, the powerplant specific mass approaches 0.2 kg/kW_e at a heat rejection temperature of ≈500 K and an enthalpy extraction ratio of ≈30%. Results for the linear MHD channel configuration display virtually identical quantitative behavior and are not shown.

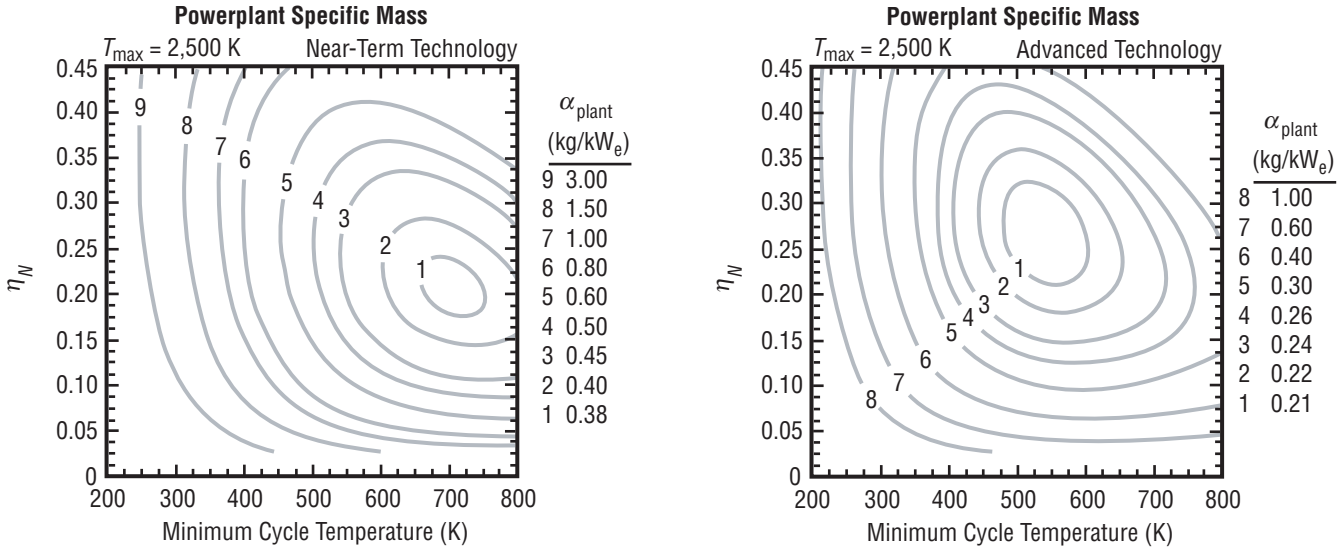

Figure 8. Specific mass characteristics of a disk MHD Brayton cycle powerplant using helium as the working fluid.

In order to keep the powerplant's circulating heat power comparable in magnitude to the generated electrical power, it is desirable to utilize the highest practical enthalpy extraction ratio consistent with specific mass optimization desires. Accepting a generator pressure ratio of $\pi_g = 8$ as an optimal value yields an enthalpy extraction ratio design value of $\eta_N = 40\%$ when $\eta_{s,g} = 70\%$. The powerplant and system specific mass characteristics for this particular case are indicated in figure 9, assuming a target radiator temperature of 500 K. Note that the propulsion system specific mass is at the 1 kg/kW$_e$ mark or less using very conservative design parameters. Also observe that the thermal efficiency now assumes a respectable value of $\eta_{th} \approx 40\%$.

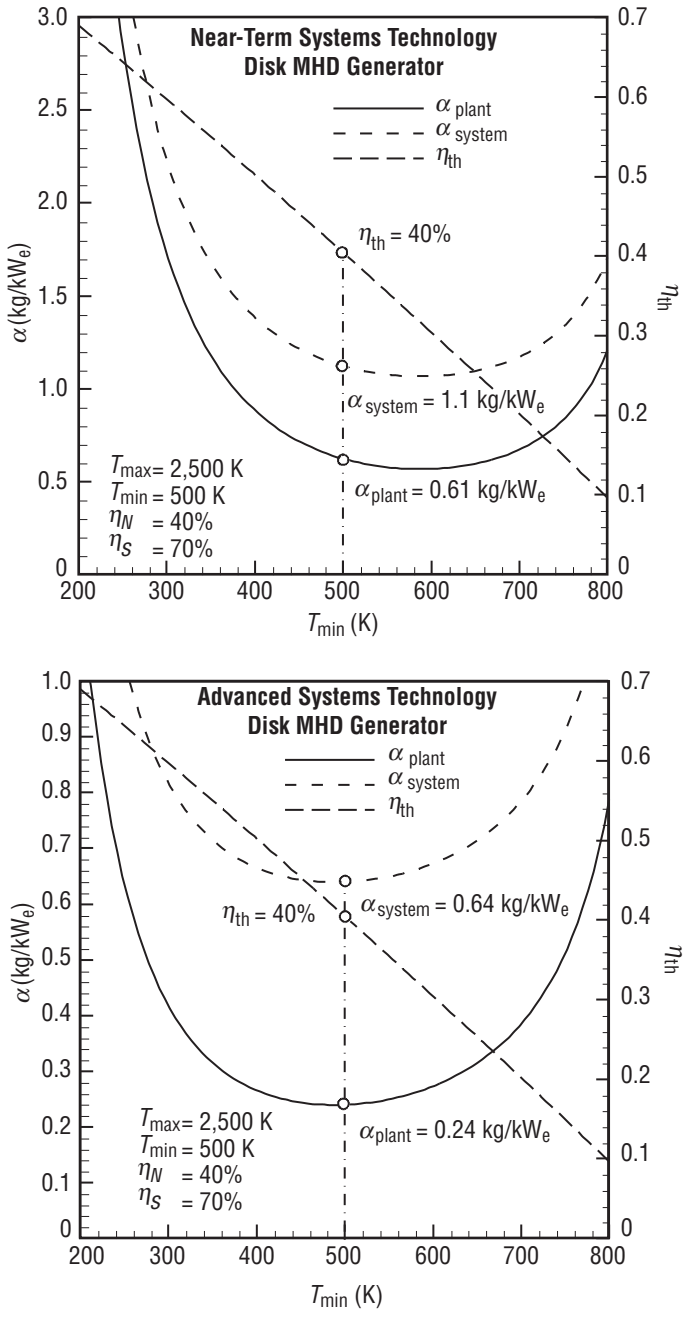

Figure 9. Disk MHD powerplant specific mass attributes for $\eta_N = 40\%$ and $\eta_{s,g} = 70\%$. The working fluid is helium.

The predicted scaling of MHD powerplant and propulsion system specific mass with net electrical power generation, under the assumption that η_N = 40%, is shown in figure 10 for peak reactor temperatures of 2,500 and 3,000 K. These estimates turn out to be in substantial agreement with the scaling results obtained by Rosa and Myrabo.[12] The scaling relationship developed by Mathematical Sciences Northwest, Inc. (MSNW) for closed-loop Brayton cycle turbogenerator systems is also shown for comparison.[20] Although the MSNW correlation indicates an economy of scale with increasing power, it is clear that the MHD Brayton cycle promises much greater payoff for a similar level of development risk.

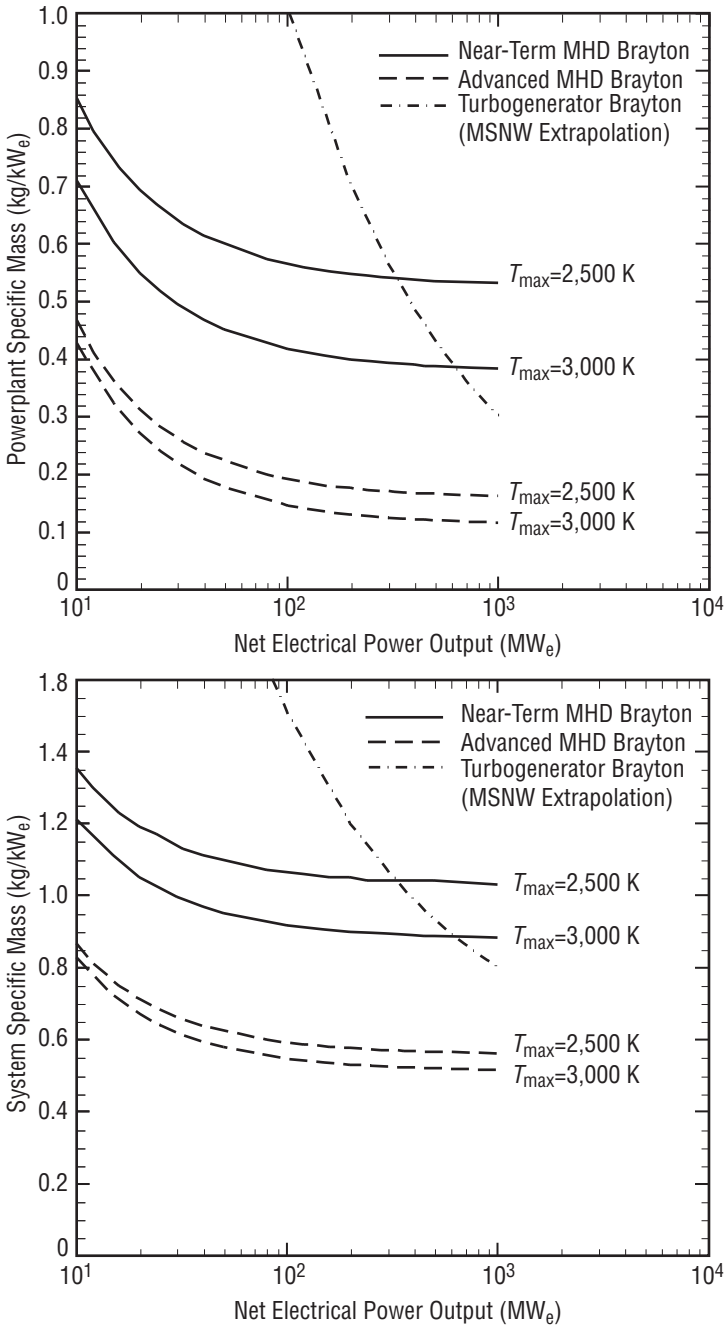

Figure 10. Scaling of MHD powerplant and propulsion system specific mass with net electrical power.

4. MAGNETOHYDRODYNAMIC TECHNOLOGY ISSUES

The success of closed-cycle nuclear MHD powerplants in space will depend on the ability to design reliable MHD generators with high-efficiency parameters. The previously discussed system analysis results, for example, depend on assumed values of 40% and 70% for the enthalpy extraction ratio and isentropic efficiency, respectively. In fact, powerplant specific mass is extremely sensitive to decreases in isentropic efficiency, and it is possible to assert that these types of installations will be competitive only if $\eta_{s,g} \geq 65\%$.[15]

A critical review of the technology reveals that the greatest hope for attaining these performance goals lies with nonequilibrium ionization Hall generators. Years of technology development effort in this arena, mainly by Japanese researchers, have yielded demonstrated efficiency parameters of $\eta_N = 30\%$ and $\eta_{s,g} = 50\%$. Clearly, this level of performance is insufficient for space installations, but these results are based on small-scale experimental facilities, which suffer severe surface-to-volume penalties. Based on detailed numerical simulations and known scaling laws, these same researchers are confident that the efficiency parameters can be raised to the necessary level at practical generator scales.

In this section, the conceptual design of a high-performance, seeded nonequilibrium disk generator is presented. Opportunities for exploiting neutron-induced ionization mechanisms are also discussed as a potential means of increasing electrical conductivity and enhancing performance and reliability.

4.1 Conceptual Design of the Nonequilibrium Disk Generator

Experience has shown that the successful design of a seeded nonequilbrium disk generator requires the simultaneous satisfaction of many conflicting restrictions. In addition to keeping the plasma stable and the isentropic efficiency high, there are practical limits on outlet Mach number, maximum wall divergence angle, maximum electric field strength, maximum electrode current density, and maximum effective electrode width.

All of these considerations are important from an engineering design perspective. For example, the outlet Mach number should be only slightly greater than unity in order to obtain good diffuser efficiency, the maximum wall divergence angle should be maintained less than 10° in order to prevent boundary layer separation, the maximum electric field strength and current density depend on available insulator and electrode materials, and the effective electrode width is always less than the actual electrode width due to current concentration.

As previously noted, Hall-configured disk generators can exhibit high isentropic efficiency only when the Hall parameter is large ($\beta > 10$), implying the need for high magnetic flux density.[17] However, it is just as important to note that nonequilibrium MHD plasmas are subject to ionization instability. This instability can create inhomogeneous gas dynamic and electrical properties and lead to severe performance degradation.[21] Past research has shown that this can be avoided in a helium plasma with fully ionized seed if the temperature is maintained in the 4,000 K $< T_e <$ 7,000 K range.[22]

To estimate the conditions necessary for satisfying this requirement, it is possible to utilize a simplified expression developed by Okuno et al. for a design parameter F defined as the ratio of the radial electric field strength to the magnetic flux density:[23]

$$F = \frac{|E_r|}{B} = \sqrt{R\left(3T_e - \frac{3+\gamma M^2}{1+\frac{\gamma-1}{2}}T_0\right)}\ , \tag{58}$$

where E_r is the radial electric field, R is the gas constant, T_e is the electron temperature, M is the Mach number, and T_0 is the stagnation temperature.

A plot of this parameter is shown in figure 11 for typical values of M and T_0. From this result, it is possible to deduce that the electric field strength per unit magnetic flux density must be in the range of 4,000 V/m·T < F < 5,000 V/m·T for the plasma to remain stable. Thus, given a permissible range on stagnation temperature and electric field strength, specification of B and E_r is sufficient to define plasma stability.

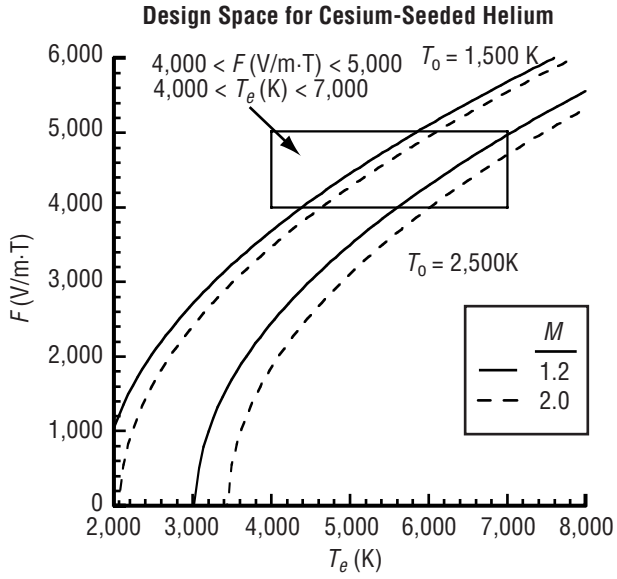

Figure 11. Variation in design parameter F with M and T_e.

Inui, Ishikawa, and Umoto have used this basic condition to develop a conceptual design methodology, which avoids the need for trial and error search procedures.[17] Using this methodology, they have developed a conceptual design for a 100-MW_{th} disk generator consistent with space power installation requirements. Their assumed design restrictions, based on practical engineering considerations, are summarized in table 4.

Table 4. MHD disk design restrictions.

Parameter	Value
$Q_{reactor}$ (MW_{th})	100
T_0 (K)	2,200
P_0 (atm)	3
r_{in} (m)	0.3
η_N (%)	40
B (T)	8
M_{exit}	1.2
θ_{max} (°)	10
$E_{r,max}$ (kV/m)	35
j_{max} (kA/m^2)	35
Effective Electrode Width (m)	0.025

Their resulting design for disk lofting is shown in figure 12 where the outlet radius is 70 cm, the inlet height is 5.8 cm, and the exit height is 8.5 cm. For detailed variation in gas dynamic and electrical properties throughout the channel, the reader is directed to the original reference.[17] The major points to note are that the plasma is stabilized at an electron temperature of $T_e \approx 5{,}000$ K and the isentropic efficiency is predicted to be $\eta_{s,g} \approx 83\%$.

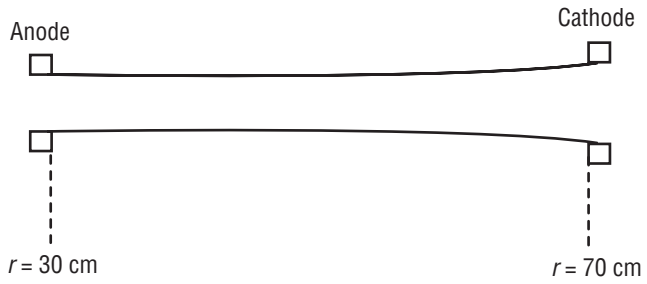

Figure 12. Design lofting for a 100-MW_{th} MHD disk generator using cesium-seeded helium working fluid.

The purpose of this conceptual design exercise is to demonstrate that MHD disk generators can be developed which exhibit the necessary performance criteria while simultaneously satisfying an array of practical engineering design restrictions. Unlike many advanced concepts, realization of nuclear MHD space power does not depend on any assumptions of idealized performance. Certainly, there are major challenges to be faced in developing this technology, but unlike many advanced concepts, one may proceed on a sound basis of realism in terms of both performance estimates and engineering feasibility.

4.2 Neutron-Induced Ionization Enhancement

Historically, closed-cycle nonequilibrium MHD research has focused on cesium-seeded inert gas working fluids. However, nuclear reactor thermal sources present opportunities for nuclear-induced ionization processes, which may greatly enhance electrical conductivity and eliminate the need to circulate condensable seed material.

In this ionization process, a working medium is either composed of or seeded with an isotope having a large neutron interaction cross section. The interaction of the neutron and the isotope results in the production of charged particles with kinetic energy, large compared to the ionization potential of the surrounding medium. These energetic charged particles then excite and ionize the surrounding molecules via collisions. Secondary ionization processes may also occur due to collisions between the liberated primary electrons and surrounding molecules. Some examples of interesting interactions with thermal neutrons are listed in table 5.

Table 5. Large cross-section neutron interactions.

Interaction	Cross Section at 0.025 eV (barns)	Kinetic Energy Release (MeV)
$^{3}He(n,p)^{3}H$	5,300	0.76
$^{10}B(n,\alpha)^{7}Li$	3,840	2.30
$^{6}Li(n,\alpha)^{3}H$	940	4.78
$^{235}U(n,ff)ff^{*}$	580	≈170

*ff denotes fission fragment

The kinetic energy released in nuclear interactions such as these is at least four orders of magnitude larger than the ionization energy of any molecule. As a result, each nuclear interaction is capable of causing thousands of ionization events, assuming all of the kinetic energy is transferred to the surrounding medium. Two mechanisms that can significantly reduce the ionization effectiveness of the nuclear products are energy loss to walls and excitation without ionization. Nonetheless, for conditions typical of MHD concepts, namely, characteristic lengths on the order of 10–100 cm and density on the order of 10^{-3}–10 STP density, each nuclear interaction can be expected to produce hundreds to thousands of ionization events. As a result, a population of free electrons can form which will enhance the electrical conductivity through electron impact excitation and ionization.

As with most innovative concepts, initial work can be traced back several decades. For example, the ^{3}He neutron interaction was first examined during the mid-1960's at AB Atomenergi in Sweden by Braun et al.[24] This experimental effort covered a temperature range of 300 to 1,600 K and density ranging from 0.25 to 1 times standard atmospheric density with a maximum thermal neutron flux of $10^{11}/cm^{2}$ sec.[25] Their measurements over this limited range of conditions, however, were not promising; i.e., 0.1 S/m, and they concluded that the nuclear-induced conductivity enhancement was insufficient for MHD energy conversion applications.

These results discouraged further study for many years. Bitteker, however, expanding on the two-temperature helium plasma model of Watanabe et al.,[26] has recently developed a kinetic model for ^{3}He which indicates that there is a regime of thermodynamic and neutron flux conditions favorable for meaningful conductivity enhancement.[27]

Bitteker's calculation for ^{3}He conductivity is shown in figure 13 as a function of relative density for different thermal neutron flux levels. It is clear from these plots that a maximum conductivity enhancement exists at some density as a function of neutron flux. At lower density, the rate of ionization is too low to produce sufficient ions to maintain the conductivity enhancement. At higher density, the rate of recombination outpaces the rate of ionization while simultaneously the charge mobility decreases, resulting in lower conductivity. Nonetheless, these graphs show that nuclear-induced ionization processes can result in very significant conductivity enhancement provided a sufficient neutron flux.

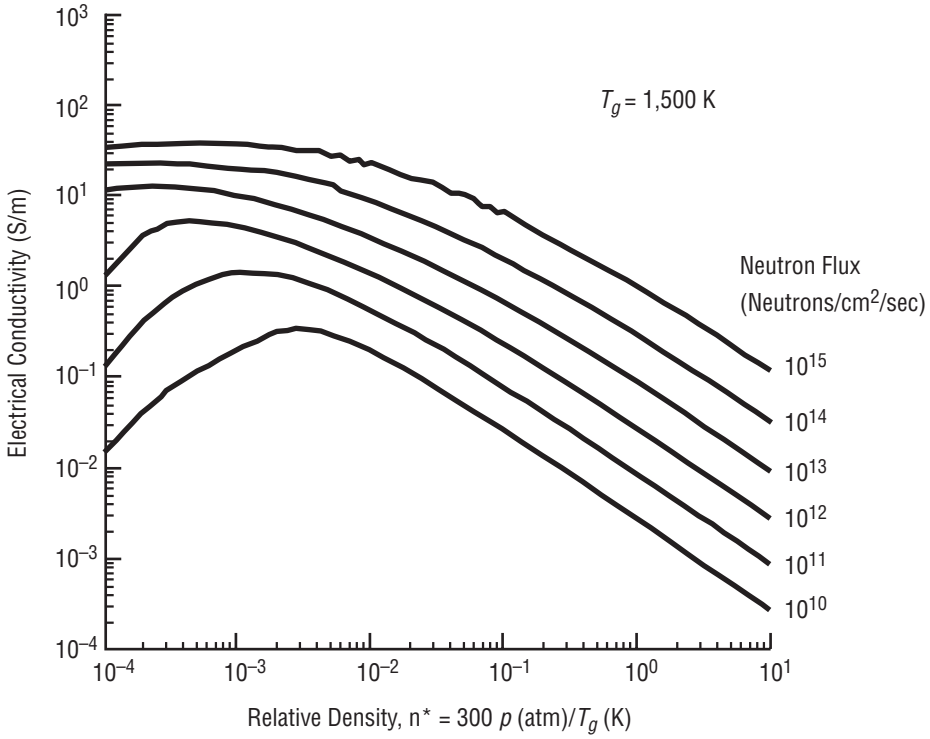

Figure 13. Computed electrical conductivity versus relative density for pure ^{3}He. Solid lines correspond to a gas temperature of 1,500 K.

Clearly, nonequilibrium conductivity enhancement requires a continuous input of ionization energy, in this case, neutrons. This fact would suggest that the entire generator must be located within the neutron field to operate. However, the rate at which the conductivity enhancement decays after the removal of the ionizing energy source is a function of the kinetics of the resulting plasma.

The ion-electron recombination process may take many routes, depending on the particular species involved, but usually some form of three-body recombination is dominant. In any case, these recombination processes are a function of the electron energy. For many gases of interest, the three-body recombination cross section decreases as the electron temperature increases above the bulk temperature, which decreases the rate of recombination, and hence, slows the decay of the conductivity enhancement. This effect becomes particularly pronounced when the electron temperature is above 0.5–1.0 eV for a typical MHD flow below a few thousand degrees Kelvin. Under these conditions, the decay of the conductivity enhancement may be decreased by orders of magnitude. This quasi-stabilized state of ionization is sometimes termed "frozen inert gas plasma."

For conditions typical of concepts using nuclear-enhanced conductivity, the duration of useful conductivity enhancement may be extended to milliseconds to tenths of seconds after exiting the ionizing energy source without any additional energy input. This time may be further extended if auxiliary electron pumping systems such as radio frequency sources are employed to maintain the electron temperature during transit.

These arguments combined with the recent kinetic calculations make a strong case for reinitiating a vigorous research program devoted to neutron-induced ionization reactions. In fact, NASA Marshall Space Flight Center staff are developing detailed research plans that address these critical technology issues on a firm experimental and theoretical basis. In the authors' opinion, the potential payoffs for nuclear MHD space power in terms of design simplicity, enhanced performance, and increased reliability more than compensate the risks associated with a focused research effort.

5. MISSION CAPABILITY ASSESSMENT

With the detailed nuclear MHD system analysis results inhand, it was of interest to examine how this technology could impact deep space mission capability. Because of its widespread benchmark appeal, the authors selected a piloted Mars mission as a baseline case, even though the technology is fundamentally suited for a much wider range of applications including interplanetary cargo transport, outer planet exploration, and routine commercial Earth-lunar transport.

In this cursory study, attention was focused on a hypothetical spacecraft using a closed-loop nuclear MHD Brayton cycle powerplant coupled to high-power electric thrusters. In order to remain consistent with the previous point design analysis, baseline calculations assumed a 100-MW_{th}, gas-cooled reactor driving a disk MHD generator having an enthalpy extraction ratio of 40% and an isentropic efficiency of 70%. This implied a thermal efficiency of 40% and a thruster input power of 40 MW_e. For near-term subsystem technology assumptions, this implied an overall propulsion system specific mass of 1.1 kg/kW_e (see fig. 9). The delivered payload was assumed to be 100 t, unless otherwise noted.

Using the widely recognized spacecraft trajectory optimization CHEBY-TOP code, several Mars trajectories were examined with respect to the 2018 Mars mission opportunities. The basis for this trajectory optimization algorithm is rooted in the early work of Melbourne at the NASA Jet Propulsion Laboratory.[28]

For all of the results reported here, the code was used to find the optimal departure date that minimized propellant usage for the outbound leg to Mars. A full round trip optimization could change the departure date and result in increased propellant requirements for the outbound journey, but the present study did not account for this effect. All trajectories were assumed to start in a 1,000-km circular Earth orbit (i.e., sufficiently high for safe operation of a nuclear reactor). The spacecraft was then spiraled out from the Earth, thrusted or coasted through heliocentric space, and spiraled into a 500-km Mars orbit.

Figure 14 shows the initial mass in low-Earth orbit (IMLEO) required to deliver a 100-t payload to Mars for trip times of 120, 150, and 180 days. The power was held constant at the design point of 40 MW_e. These results show that high-power thrusters with specific impulse capabilities between 5,000 and 8,000 sec are attractive for this mission scenario. Within this specific impulse range, it is observed that the payload can account for as much as half of the IMLEO. The outbound trajectories for the 180- and 120-day transits are shown in figure 15.

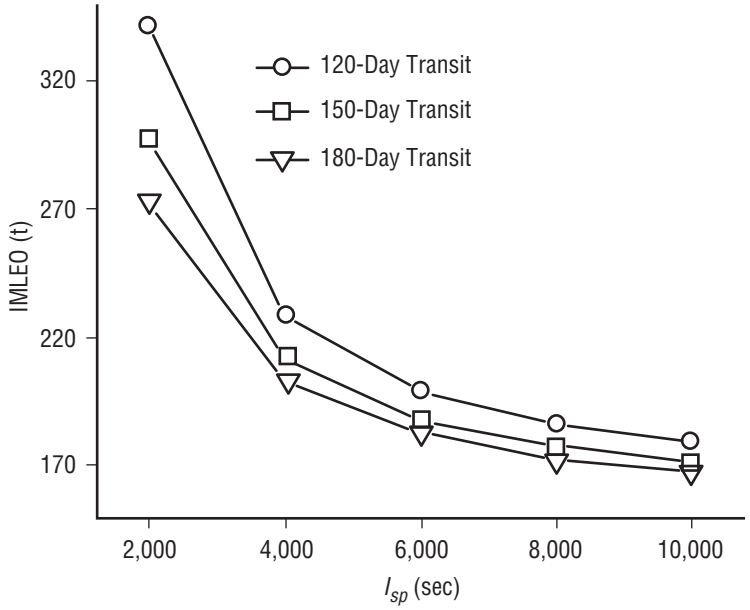

Figure 14. IMLEO as a function of specific impulse for a 40-MW_e nuclear MHD space power installation delivering a 100-t payload to Mars.

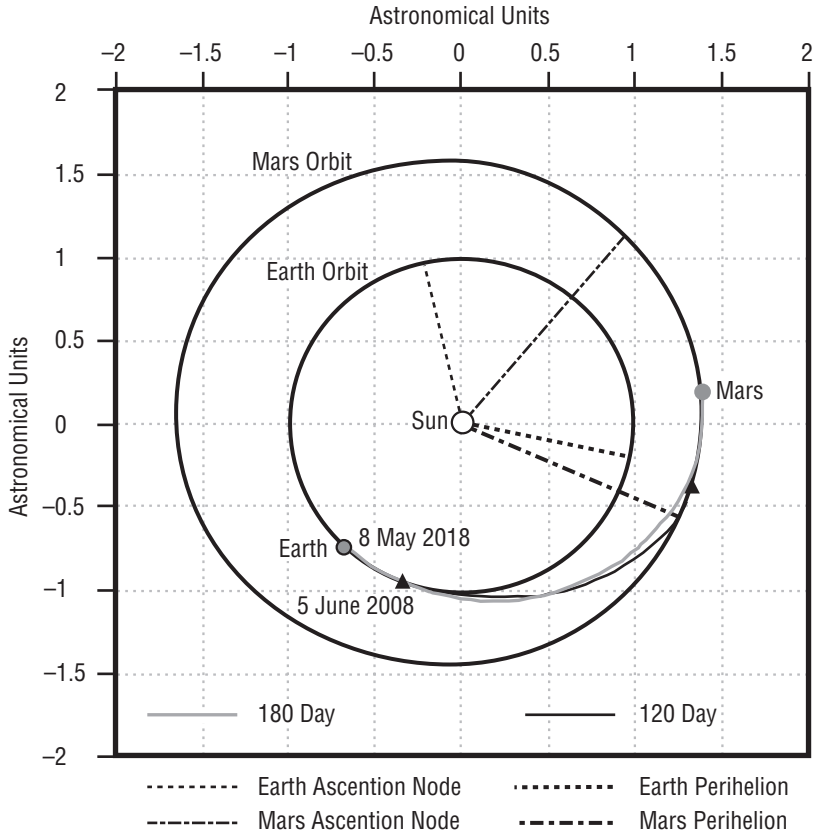

Figure 15. Optimal trajectories for 120- and 180-day transits. Assumes 100-t payload and 40-MW_e thruster power.

Because the CHEBY-TOP code also had the capability of determining the optimal power for a given system configuration, it was of additional interest to examine those predictions for the 100-t payload. The predicted optimal power characteristics are shown in figure 16 along with the corresponding system specific mass and IMLEO. Here, the optimal power for delivering 100 t in 120 days starts out at 13.2 MW_e, at a specific impulse of 2,000 sec, and climbs to 30.6 MW_e, at a specific impulse of 10,000 sec. Thus, the 40-MW_e point design is substantially greater than the optimal thruster power requirement. Simply put, the power supply is oversized for the stated mission parameters.

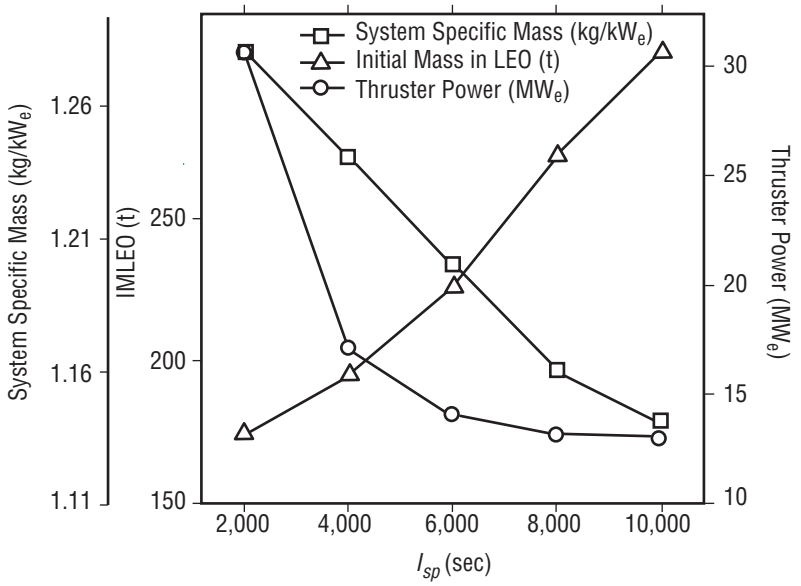

Figure 16. Optimal power characteristics of a nuclear MHD space power installation for a 100-t payload.

The 40-MW_e installation point design could be used optimally in two alternative ways: faster trip times and/or larger payloads. For example, if the trip time is held constant at 120 days and the payload is allowed to vary so that thruster power is optimized at 40 MW_e, the results shown in figure 17 are obtained. In this case, it is possible to deliver 293 t to Mars in 120 days using a thruster having a specific impulse of 2,000 sec; however, the IMLEO, in this case, is a monstrous 880 t. For a thruster having a specific impulse of 10,000 sec, the delivered payload drops to 132 t, but the IMLEO becomes much more reasonable at 225 t. Note that any high-power thruster technology having specific impulses >6,000 sec will yield a payload fraction (mass of payload/IMLEO) greater than 0.56. This is a very attractive feature for fast 120-day transits.

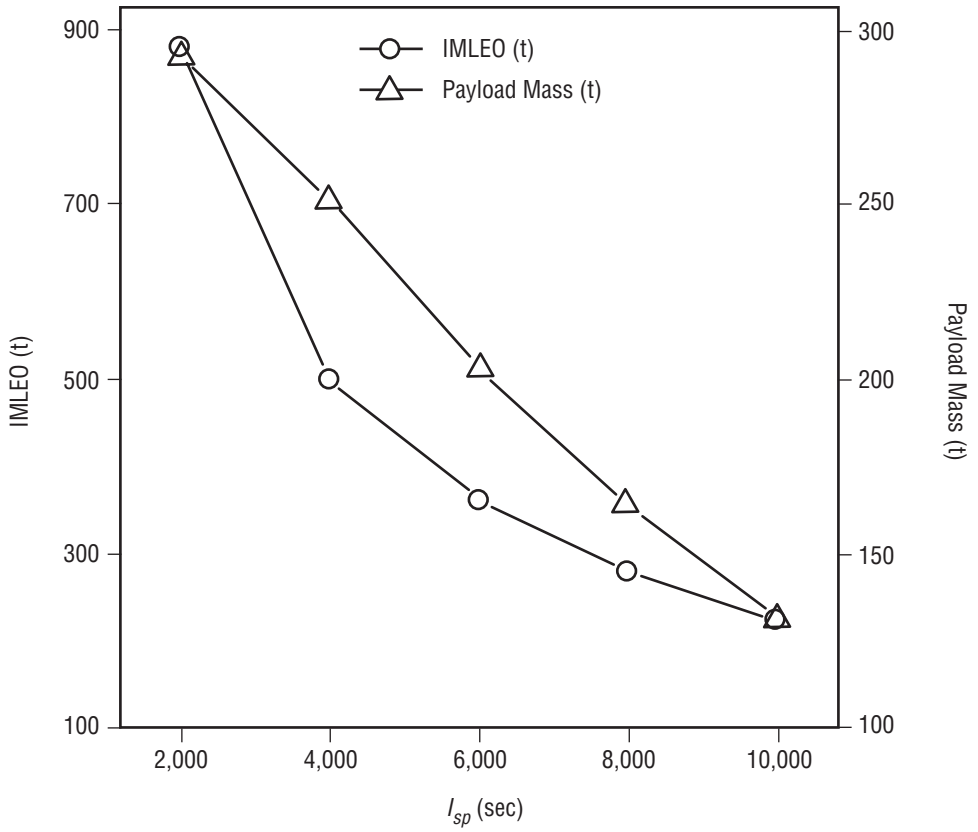

Figure 17. Optimized payload for a 40-MW_e nuclear MHD space power installation.

While admittedly incomplete, these mission analyses indicate the enormous potential of nuclear MHD space power installations when coupled to high-power electric thrusters. The authors strongly emphasize that these mission capabilities are based on a practical systems level assessment with conservative projections for subsystem technology development.

6. CONCLUSIONS

After thoughtful examination of deep space propulsion requirements and potential technological solutions, the authors concluded that nuclear fission reactors coupled with MHD generators could serve as suitable low specific mass powerplants for high-power electric propulsion systems. These systems display the necessary energy density requirements while also remaining entirely within the realm of current engineering feasibility. The technological development risk for multimegawatt installations is only slightly greater than for turbogenerator-based powerplants, yet the potential payoff is immense—an order of magnitude or more decrease in system specific mass.

Based on this line of reasoning, the authors pursued a preliminary system analysis of multimegawatt nuclear electric propulsion (NEP) in which a gas-cooled nuclear reactor is used to drive an MHD generator in a closed-loop Brayton cycle. The primary purpose of this exercise was to demonstrate that the necessary subsystem technologies either currently exist or have a basis in the existing technology base with clear development paths for attaining the required performance attributes.

This was accomplished by using a thermodynamic cycle analysis in context with a thorough system analysis to explore the available design space. The results of this analysis indicated the appropriate operating regime as well as the range of subsystem component performance needed to make the system viable.

The major technological hurdles may be summarized as follows: Develop reliable, long-life, high-temperature fissile fuel elements; demonstrate an increase in the nonequilibrium MHD generator enthalpy extraction ratio from 30% to 40% and isentropic efficiency from 50% to 70%; develop efficient high-power (megawatt class) electric thruster technologies; and demonstrate that the entire system can attain a useful operating lifetime. A major advantage here is that the higher performance translates into a shorter lifetime requirement (megawatt class) i.e., days or months instead of years. It should be noted that improvements in space radiator technology would also be immensely beneficial, but adequate systems could be developed using the existing state of the art.

Based on these results, the authors conclude that MHD NEP technology offers a path for high-payoff, near-term realization with limited development risk. As such, the authors recommend that vigorous technology development steps be undertaken.

REFERENCES

1. Sackheim, R.; Van Dyke, M.; Houts, M.; Poston, D.; Lipinski, R.; Polk, J.; and Frisbee, R.: "In-Space Nuclear Power as an Enabling Technology for Deep Space Exploration," AIAA Paper 2000–3881, American Institute of Aeronautics and Astronautics, 2000.

2. Rosa, R.J.: "An Electromagnetic Rocket System of High Specific Thrust," Research Report No. 103, Avco Everett Research Laboratory, April 1958.

3. Rosa, R.J.: "Propulsion System Using a Cavity Reactor and Magnetohydrodynamic Generator," *ARS Journal*, Vol. 31, pp. 884–889, July 1961 (see also, ARS Report 1519–60).

4. Rosa, R.J.: "Magnetohydrodynamic Generators and Nuclear Propulsion," *ARS Journal*, Vol. 32, pp. 1221–1230, August 1962.

5. Rosa, R.J.: "A Discussion of Nuclear Propulsion Using MHD Conversion Techniques," Advanced Nuclear Propulsion Conference, Los Alamos National Laboratory, April 1964 (see also, AMP 153, Avco Everett Research Laboratory, February 1965).

6. Rosa, R.J.: "Radiating Space Powerplants Using the MHD Generator," AMP 148, Avco Everett Research Laboratory, February 1965.

7. Rosa, R.J.: "A High Temperature Radiating Vapor Cycle," *Seventh Symposium on Engineering Aspects of MHD*, Princeton, NJ, February 1966.

8. Rosa, R.J.: "Unconventional Propulsion Systems," AAS Paper No. 67–131, American Astronautical Society, 13th Annual Meeting, Dallas, TX, May, 1–3, 1967.

9. Seikel, G.R.; and Nichols, L.D.: "Potential of Nuclear MHD Electric Power Systems," *J. of Spacecraft and Rockets*, Vol. 9, pp. 322–326, May 1972.

10. Thom, K.; and Schwenk, F.C.: "Gaseous-Fuel Reactor Systems for Aerospace Applications," *J. of Energy*, Vol. 1, pp. 267–276, September–October 1977.

11. Rosa, R.J.: "Magnetohydrodynamics Applied to Aerospace and Deep Space Propulsion," AIAA Paper No. 82–1212, American Institute of Aeronautics and Astronautics, 1982.

12. Rosa, R.J.; and Myrabo, L.N.: "Ultraperformance Closed-Cycle Gas Core Reactors for Orbit Raising," *Orbit-Raising and Maneuvering Propulsion—Research Status and Needs*, AIAA Progress in Astronautics and Aeronautics, Vol. 89, L.H. Caveny (ed.), pp. 460–476, AIAA, New York, NY, 1983.

13. Dias, N.; Anghaie, S.; Dugan, E.T.; and Maya, I.: "Gas Core Reactor Concepts and Technology," AIAA Paper 91–3582, American Institute of Aeronautics and Astronautics, 1991.

14. Maya, I.; Anghaie, S.; Diaz, N.J.; and Dugan, E.T.: "Ultra Temperature Vapor Core—MHD System for Space Nuclear Electric Power," AIAA Paper 91–3632, American Institute of Aeronautics and Astronautics, 1991.

15. Slavin, V.S.; Danilov, V.V. ; and Kraev, M.V.: "Space Transport System on the Basis of MHD Generator and Electric Rocket Engine," *Proceedings of the International Conference on MHD Power Generation and High Temperature Technologies 1999*, Vol. II, Beijing, PRC, pp. 694–707, October 12–15, 1999.

16. Holman, R.R.: "A Critique of NERVA-Based Nuclear Reactor Design and Performance for MMW Space Propulsion Applications," *Space Nuclear Power Systems 1987*, Vol. 7, M.S. El-Genk and M.D. Hoover (eds.), Orbit Book Company, Malabar, FL, pp. 527–531, 1988.

17. Inui, Y.; Ishikawa, M.; and Umoto, J.: "Proposal for New Conceptual Design Method of Nonequilibrium Disk MHD Generator," *31st Symposium on Engineering Aspects of MHD*, Whitefish, MT, pp. III.1.1–III.1.8, 1993.

18. Rosa, R.J.: *Magnetohydrodynamic Energy Conversion*, Revised Printing, Hemisphere Publishing, New York, NY, 1987.

19. Chang-Diaz, F.; Squire, J.; Bering, E.; George, J.; Ilin, A.; and Petro, A.: "The VASIMR Engine Approach to Solar System Exploration," AIAA Paper No. 2001–0960, American Institute of Aeronautics and Astronautics, 2001.

20. Taussig, R.; and Christiansen, W.: "Design Investigation of Solar-Powered Lasers for Space Application," Contract No. NAS3–21134, Mathematical Sciences Northwest, Inc., Bellevue, WA, November 1978.

21. Kerrebrock, J.L.: "Nonequilibrium Ionization Due to Electron Heating: I. Theory," *AIAA J.*, Vol. 2, p. 1072, 1964.

22. Nakamura, T.; and Riedmuler, W.: "Stability of Nonequilibrium MHD Plasma in the Regime of Fully Ionized Seed," *AIAA J.*, Vol. 12, p. 661, 1974.

23. Okuno, Y.; Okamura, T.; and Shioda, S.: "Feasibility of a Disk Type Nonequilibrium MHD Generator With Subsonic Flow," *Transactions of IEE of Japan*, Vol. 110–B, p. 603, 1990.

24. Braun, J.; Nygard, K.; and Witalis, E.: "On Plasma Through Neutron Irradiation," *International Symposium on MHD Electrical Power Generation*, Paris, France, Vol. 1, pp. 179–194, 1964.

25. Braun, J.; and Nygard, K.: "Measurement of the Electrical Conductivity of ^{3}He Plasma Induced by Neutron Irradiation," *Proceedings of the Symposium on MHD Electrical Power Generation*, Vienna, Austria, pp. 557–570, 1966.

26. Watanabe, Y.; Appelbaum, J.; and Maya, I.: "Two-Temperature Model of Helium Plasmas with Fast-Ion Induced Nonequilibrium Ionization," AIAA Paper 90–1613, American Institute of Aeronautics and Astronautics, 1990.

27. Bitteker, L.: "Nuclear-Induced Electrical Conductivity in ^{3}He," *J. App. Phys.*, Vol. 83, No. 8, pp. 4018–4023, 1998.

28. Melbourne, W.G.: "Interplanetary Trajectories and Payload Capabilities of Advanced Propulsion Vehicles," NASA Jet Propulsion Laboratory Technical Report No. 32–68, March 1961.

REPORT DOCUMENTATION PAGE

Form Approved
OMB No. 0704-0188

1. AGENCY USE ONLY *(Leave Blank)*	2. REPORT DATE	3. REPORT TYPE AND DATES COVERED
	October 2001	Technical Publication

4. TITLE AND SUBTITLE

Prospects for Nuclear Electric Propulsion Using Closed-Cycle Magnetohydrodynamic Energy Conversion

5. FUNDING NUMBERS

6. AUTHORS

R.J. Litchford, L.J. Bitteker, and J.E. Jones

7. PERFORMING ORGANIZATION NAMES(S) AND ADDRESS(ES)

George C. Marshall Space Flight Center
Marshall Space Flight Center, AL 35812

8. PERFORMING ORGANIZATION REPORT NUMBER

M–1027

9. SPONSORING/MONITORING AGENCY NAME(S) AND ADDRESS(ES)

National Aeronautics and Space Administration
Washington, DC 20546–0001

10. SPONSORING/MONITORING AGENCY REPORT NUMBER

NASA/TP—2001–211274

11. SUPPLEMENTARY NOTES

Prepared for the Advanced Space Transportation Program, Space Transportation Directorate

12a. DISTRIBUTION/AVAILABILITY STATEMENT

Unclassified-Unlimited
Subject Category 20
Standard Distribution

12b. DISTRIBUTION CODE

13. ABSTRACT *(Maximum 200 words)*

Nuclear electric propulsion (NEP) has long been recognized as a major enabling technology for scientific and human exploration of the solar system, and it may conceivably form the basis of a cost-effective space transportation system suitable for space commerce. The chief technical obstacles to realizing this vision are the development of efficient, high-power (megawatt-class) electric thrusters and the development of low specific mass (<1 kg/kW_e) power plants. Furthermore, comprehensive system analyses of multimegawatt class NEP systems are needed in order to critically assess mission capability and cost attributes. This Technical Publication addresses some of these concerns through a systematic examination of multimegawatt space power installations in which a gas-cooled nuclear reactor is used to drive a magnetohydrodynamic (MHD) generator in a closed-loop Brayton cycle. The primary motivation for considering MHD energy conversion is the ability to transfer energy out of a gas that is simply too hot for contact with any solid material. This has several intrinsic advantages including the ability to achieve high thermal efficiency and power density and the ability to reject heat at elevated temperatures. These attributes lead to a reduction in system specific mass below that obtainable with turbine-based systems, which have definite solid temperature limits for reliable operation. Here, the results of a thermodynamic cycle analysis are placed in context with a preliminary system analysis in order to converge on a design space that optimizes performance while remaining clearly within established bounds of engineering feasibility. MHD technology issues are discussed including the conceptual design of a nonequilibrium disk generator and opportunities for exploiting neutron-induced ionization mechanisms as a means of increasing electrical conductivity and enhancing performance and reliability. The results are then used to make a cursory examination of piloted Mars missions during the 2018 opportunity.

14. SUBJECT TERMS

nuclear, electric, propulsion, power, magnetohydrodynamics, spacecraft, Mars mission

15. NUMBER OF PAGES

52

16. PRICE CODE

17. SECURITY CLASSIFICATION OF REPORT	18. SECURITY CLASSIFICATION OF THIS PAGE	19. SECURITY CLASSIFICATION OF ABSTRACT	20. LIMITATION OF ABSTRACT
Unclassified	Unclassified	Unclassified	Unlimited